Spring 5-2018

# Temporal and Spatial Variability of Oxygen Levels in Upwelled Waters Along the Southern California Coast

Todd Xavier Thoman
*University of Maine*

# TEMPORAL AND SPATIAL VARIABILITY OF OXYGEN LEVELS IN UPWELLED WATERS ALONG THE SOUTHERN CALIFORNIA COAST

by

Todd Xavier Thoman

A Thesis Submitted in Partial Fulfillment
of the Requirements for a Degree with Honors
(Marine Sciences)

The Honors College

University of Maine

May 2018

Advisory Committee:

Dr. Andrew Thomas, Professor, School of Marine Sciences
Dr. Cristina Arrigoni Martelli, Preceptor, Honors College
Dr. Emmanuel Boss, Professor, School of Marine Sciences
Dr. Damian Brady, Associate Research Professor, School of Marine Sciences
Dr. Mark Wells, Professor, School of Marine Sciences

# ABSTRACT

The overall goal of this study is to quantify interannual trends in oxygen concentrations and their spatial variability in the coastal Pacific Ocean off the southern coast of California, and to examine their relationship to concurrent hydrographic properties. The study focuses on trends within the upper 500 meters of the water column to indicate changes in seasonally upwelled waters over time. The analysis uses the publicly-available CalCOFI bottle cast data gathered and distributed by Scripps Institute. At each station, data include oxygen concentration and hydrographic information, such as potential density, depth, temperature, and salinity. This study utilizes data from 30.35° N and 34.21° N. Using MATLAB, data were bin-averaged and interpolated into quarterly time series at 24 stations and at standard depths. Figures were constructed to visualize latitudinal variability and cross-shelf variability of seasonal and interannual oxygen concentrations throughout the water column. Overall trends of oxygen at both standard depths and fixed density surfaces were approximated by a non-parametric linear fit. Observed multi-year trends in oxygen concentration are quantified and compared to those evident in hydrographic data under identical methods. Declining oxygen concentrations occur across the entire study region, peaking in the range of the California undercurrent. Deoxygenation rates maximize at equivalent magnitudes when viewed by both depth and density, reinforcing prior assertions that increasing advection of low oxygen Pacific Equatorial waters into the system is a strong driver of deoxygenation. On isopycnals, oxygen concentrations trends track best with salinity, suggesting salinity trends may be usable to predict oxygen trends.

ACKNOWLEDGEMENTS

The author would like to thank the Scripps Institute of the University of California San Diego and the associated California Cooperative Oceanic Fisheries Investigation responsible for the collection and public distribution of the chemical and hydrographic data utilized in this study. The author would additionally like to thank the Pacific Fisheries Environmental Laboratory of the National Oceanic and Atmospheric Administration for providing data related to the upwelling index of the California coast.

Moreover, the author would like to thank Dr. Andrew Thomas for advising and guiding this project from conceptualization to completion. The author would also like to thank the following individuals for reviewing and offering revisions to this work and the associated Honors Reading List: Dr. Andrew Thomas, Dr. Emmanuel Boss, Dr. Mark Wells, and Dr. Cristina Arrigoni Martelli.

TABLE OF CONTENTS

TABLE OF FIGURES

# INTRODUCTION

Over the past few decades, deoxygenation has been noted throughout many of the world's oceans (Stramma *et al*., 2010). Low oxygen levels, presenting primarily as hypoxia (oxygen concentrations < 2 ml/L) (McClatchie *et al*., 2010; Stramma *et al*., 2010), can act as a defining feature of the spatial distribution of organisms within marine environments (McClatchie *et al*., 2010 & Gilly *et al*., 2013). In areas with oxygen minimum zones, subsurface features characterized by either low oxygen concentrations or saturations (Gilly *et al*., 2013), impacts become visible through vertical limits of available habitat for many pelagic species, including commercially relevant species of fish (McClatchie *et al*., 2010). As such, deoxygenation trends attract a significant amount of attention. The occurrences of such trends have been tied to numerous sources, including shoaling oxygen minimum layers (Bograd *et* al., 2008; McClatchie *et al*., 2010; Gilly *et al*., 2013), changes in source waters (Connolly *et al*., 2010 & Bograd *et al*., 2015), changes in upwelling extent (Connolly *et al*., 2010), and increased respiration (Connolly *et al*., 2010).

Heavy deoxygenation trends have appeared across much of the world, including tropical regions, subtropical regions (Stramma *et al*., 2010), and many eastern boundary current systems (Stramma *et al*., 2010 & Gilly *et al*., 2013). Among the eastern boundary current systems, deoxygenation along the coast of California has been heavily studied (Bograd *et al*., 2008; McClatchie *et al*., 2010; Meinvielle and Johnson, 2013; Bograd *et al*., 2015; Nam *et al*., 2015). Deoxygenation and associated shoaling of the oxygen minimum zones appeared in this region in the mid-1980s (Bograd *et* al., 2008 &

McClatchie *et al*., 2010). Within and directly north of the Southern California Bight, deoxygenation patterns have been well studied due to the availability of a historical and detailed data set. The region features a peak in deoxygenation rates in the vicinity of the California Undercurrent, as indicated by both density and approximate depth (Bograd *et al*., 2008; Meinvielle and Johnson, 2013; Bograd *et al*., 2015). Moreover, the region displays positive trends in spiciness, a calculated variable defined by temperature and salinity along lines of equal density (Meinvielle and Johnson, 2013), suggesting stronger inputs of Pacific Equatorial water within the California Current system (Meinvielle and Johnson, 2013; Nam *et al*., 2015).

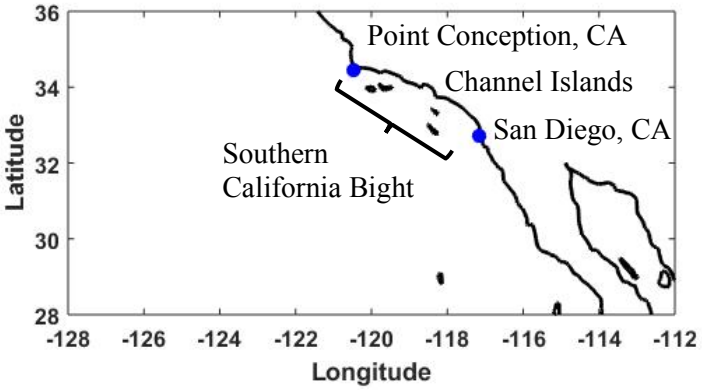


**Figure 1.** Study area along the southern California coast with relevant locations and geographic features.

The southern coast of California sits within the California Current system. This region is dominated by two primary currents – the California Current and the California Undercurrent (Lynn and Simpson, 1987). The California Current exists as a surficial, primarily equatorward flow of water fed by Pacific Subarctic Upper water and Eastern North Pacific Central water (Lynn and Simpson, 1987). The California Undercurrent runs poleward primarily at depths of around 200 to 300 meters (Lynn and Simpson, 1987 & Nam *et al*., 2015). The California Undercurrent derives primarily from Pacific Equatorial water (Lynn and Simpson, 1987). Over time, this water dilutes with Pacific Subarctic Upper Water along its path (Lynn and Simpson, 1990 & Nam *et al*., 2015). As

an eastern boundary current, the California Current system is characterized by seasonal upwelling that brings subsurface water to the surface along coastal regions, driven by equatorward wind stress (Bray *et al*., 1999).

South of Point Conception, CA, inward curvature of the coast creates a feature known as the Southern California Bight (Fig. 1). Within this region, circulation patterns differ from those along the open coast, especially with regard to the California Current. The California Current exhibits annual shifts away from shore through the fall and winter and inshore in spring months (Bray *et al*., 1999). Within the Bight, this shift appears more dramatic. During the spring, elevated flow rates and inshore movement of the California Current allow for equatorward flow in the Bight; however, from summer through winter, offshore movement of the California Current opens the Bight to a returning poleward flow of California Current waters (Bray *et al*., 1999). Additionally, the curvature of the Bight, accompanied by island chains within the Bight (Fig. 1), has been noted to decrease wind-driven upwelling responses, reflected in shallower, weaker offshore Ekman transport along the interior of the Southern California Bight (Caldiera and Marchesiello, 2002). In total, the geometry of the Bight generates significant alterations to the California Current system with regards to latitude and cross-shelf structure.

In this study, we utilize oxygen concentration and hydrographic data from 24 stations along four lines sampled quarterly as part of the California Cooperative Oceanic Fisheries Investigation (CalCOFI) to verify and expand upon the spatial and temporal trends in oxygen concentration observed by Bograd *et al*. (2008). Then, we break down

trends in spiciness to its component parts to determine which physical characteristic serves as a better indicator of oxygen trends within the system.

# DATA AND METHODS

## Data

Data for this study were collected as part of the California Cooperative Oceanic Fisheries Investigation project. These data are publicly available for use through the CalCOFI data resources website (http://new.data.calcofi.org/index.php/reporteddata). This study utilizes data from the Hydrographic Bottle Cast data set, which consists of data collected on cruises focused along the California coast beginning in 1949. Beginning in the mid-1980s, data collection increased in consistency, cataloguing data quarterly at standard stations between Point Conception, CA and San Diego, CA (see Fig. 1) in five lines running roughly perpendicular to the coast (Fig. 2). Here, patterns and trends in the data from 1988 to 2016 are the focus.

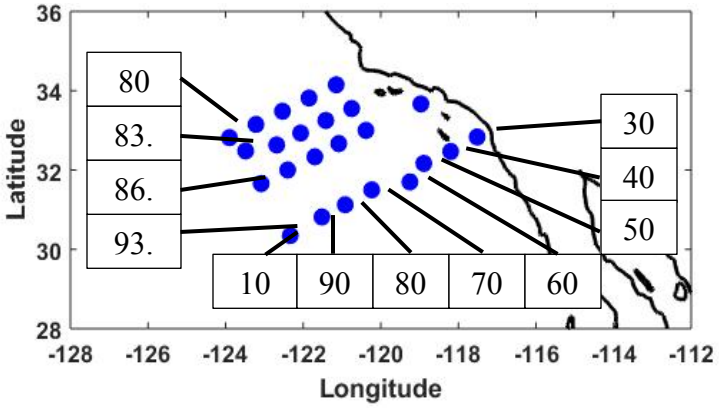


**Figure 2.** Map of station locations used in this study. The second term of the station name increases moving away from the coast. From north to south, the lines are designated line 80, line 83.3, Line 86.7, and line 93.3.

During the study period, bottle casts at each station include up to 20 bottles deployed at depths down to 525 meters (CalCOFI, 1989 & CalCOFI, 2016). Earlier casts, utilized here to calculate climatological means, could reach depths exceeding 1000 meters. CalCOFI data sets distribute both observed data and interpolated data to represent a set of standard depths (CalCOFI, 1989). Thermometers, both protected and unprotected, were initially utilized to catalog temperature and pressure (CalCOFI, 1989);

after 1993, a Seabird Conductivity-Temperature-Depth (CTD) sensor became the default mode to observe these variables (CalCOFI, 2016). Salinity and dissolved oxygen data were determined on board the ship from bottle samples using Practical Salinity Scale calculations of salinometer outputs and adjusted Winkler Titrations, respectively (CalCOFI, 1989 & CalCOFI, 2016). In time, CTD data became a precautionary check for salinity data accuracy (CalCOFI, 2016).

## Data Management

Profiles obtained via the CalCOFI database were first interpolated linearly to standard depths (10 m, 20 m, 30 m, 50 m, 60 m, 75 m, 90 m, 100 m, 125 m, 150 m, 200 m, 250 m, 300 m, 400 m, 500 m, 600 m, 700 m, 800 m, 900 m, 1000 m). Due to the consistent data presentation of the CalCOFI data reports, most data were interpolated to standard points before the data were made publicly available (CalCOFI, 1989). As such, depths selected for this study coincided with commonly available depths within the data, ranging from ten meters to 500 meters, with higher data density nearer the surface.

Data for oxygen concentration, temperature, salinity, and potential density in each year were then temporally averaged into quarterly profiles at each of 24 selected stations along the lines 80, 83.3, 86.7, and 93.3 (Fig. 2). For this study, quarters were centered on the most frequently sampled months – January, April, July, and October.

Climatological mean quarterly profiles were then constructed for each variable at each station by averaging all available profiles of a quarter over all years into a single mean profile. These climatological means were calculated using data available back to 1950 to provide a greater historical view of the climatological mean. Quarterly anomaly profiles for each variable in the study period (1988-2016) were then calculated by

subtracting the climatological mean profiles of the respective variable, quarter, and station from each available profile.

Finally, density-interpolated anomaly profiles were generated for the data set for the period of 1988 to 2016. Each depth-interpolated anomaly profile underwent density-based linear interpolation to six standard potential densities. These potential density values ranged from 25.5 $kg/m^3$ to 26.75 $kg/m^3$ in increments of 0.25 $kg/m^3$.

For each of six standard depths (10 m, 30 m, 50 m, 100 m, 200 m, and 500m) and on each standard potential density (isopycnal), a linear trend over time was determined. Due to unknown statistical properties of the anomaly series, potentially capable generating or exaggerating poor correlation under a traditional least-squared regression, linear trends were determined via the non-parametrical Sen's slope method.

## Data Visualization

Climatological trends in each variable are visualized by line as quarterly cross-shelf contours. Anomalies of each variable are plotted at three stations for each line. Stations are chosen as the most nearshore station of each line used within the study plus two more stations shifted offshore at roughly equivalent distances. These distances are maintained between lines by following station numbers, such that each successive station within a line has a number 20 greater than the previous (i.e. – 90 30, 90 50, 90 70). Anomalies are plotted at these stations, tracking anomaly values at six standard depths over the course of the study. It is against this type of temporal display that the Sen's slope is calculated. Sen's slopes for each depth at each of the 24 stations are then mapped to visualize spatial patterns. In order to examine relationships between oxygen and hydrographic variables, Sen's slopes at equal depths for oxygen concentrations and

either temperature or salinity are regressed against one another and a linear trend is fit using a least-squared regression. From this linear regression, correlation coefficients are calculated. Identical methods are performed along the six standard isopycnals.

# RESULTS

## Climatological Patterns

All four lines used in this study are characterized by seasonal upwelling, strongest in the spring, as isopycnals tilt upward toward shore (Fig. 3). Lines 80 and 83.3 show signs of weaker upwelling heading into summer. In lines 86.7 and 93.3, strong subsurface (below ≈200 m) depression of isopycnals appears in nearshore stations from summer to winter. At all lines, potential density decreases moving away from shore, as isopycnals deepen. Moreover, density decreases moving south. Near-surface densities follows a seasonal pattern, increasing in winter and spring and decreasing in summer and

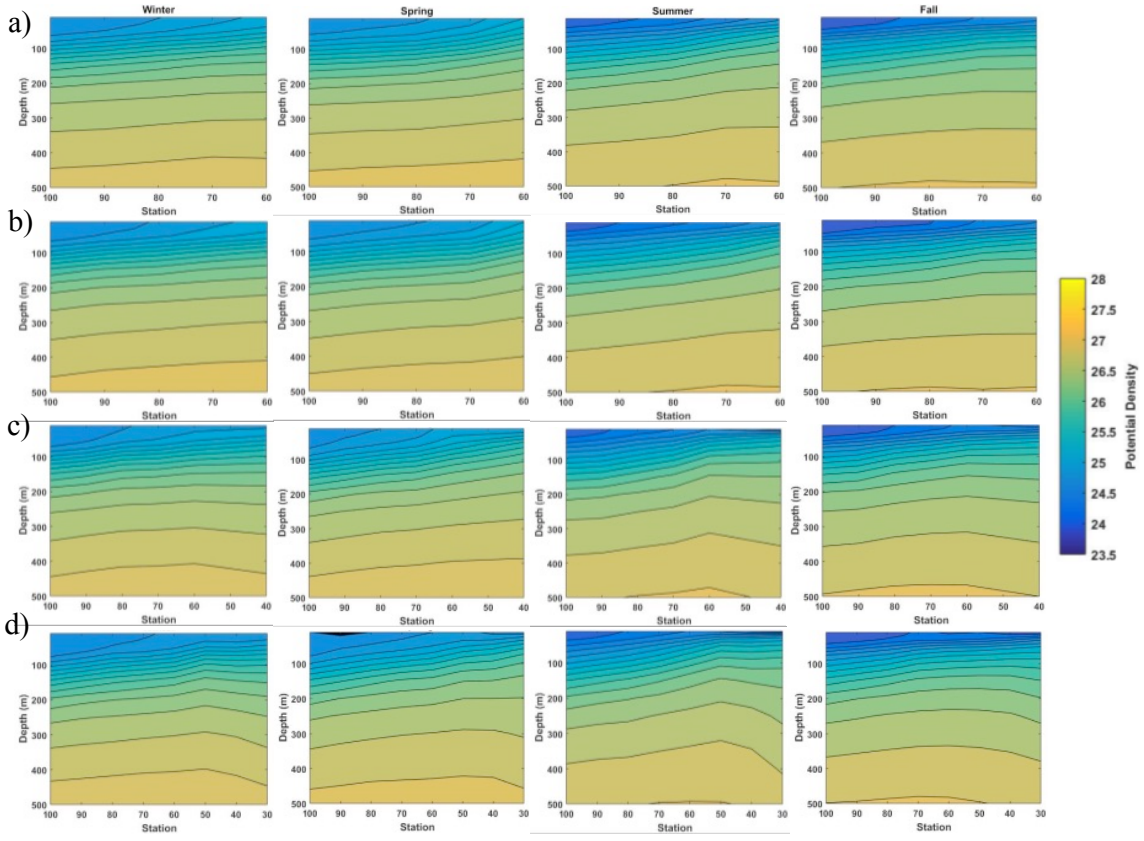


**Figure 3.** Climatological, seasonal contours of cross-shelf vertical potential density structure in the upper 500 meters from 1950 to 2016 along lines a) 80, b) 83.3, c) 86.7, and d) 93.3.

fall. Temperatures (Fig. A1) show expected trends under these density patterns, rising away from the upwelling region near shore and peaking during the heating of summer and fall (Fig. A1). Salinity shows less variability throughout the year than the other variables (Fig. A2). The most obvious trend appears with latitude. Nearshore salinities increase to the south, suggesting weaker advection of relatively fresh California Current waters to nearshore southern stations.

Climatological oxygen concentrations mirror the cross-shelf patterns observed in the climatological hydrography, including showing nearshore upwelling patterns in the spring. Concentrations peak in the spring (Fig. 4) and decline into summer, with

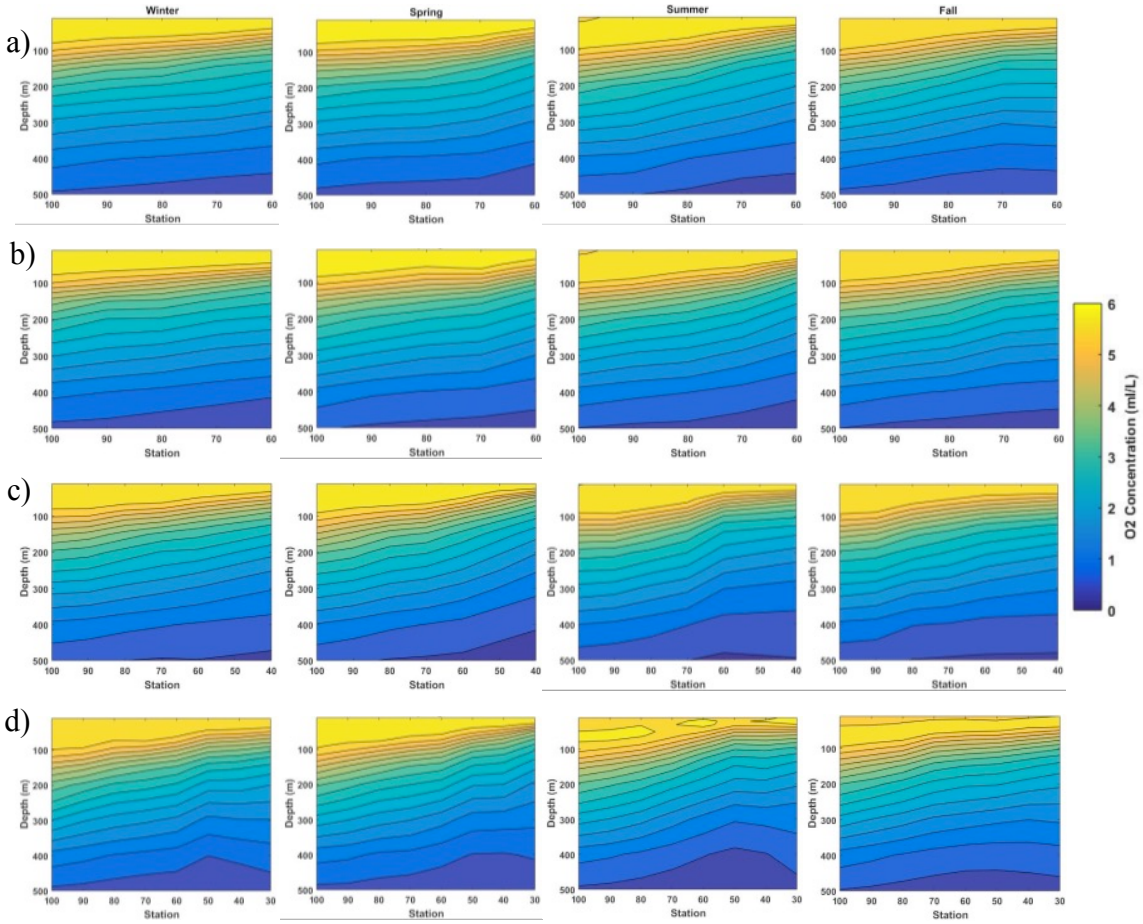


**Figure 4.** Climatological, seasonal contours of cross-shelf vertical oxygen concentrations in the upper 500 meters from 1950 to 2016 along lines a) 80, b) 83.3, c) 86.7, and d) 93.3.

maximum levels appearing as subsurface maxima at outer stations of lines 80 and 86.7. A subsurface oxygen maximum also appears at line 93.3; however, the feature is noticeably nearer to the shore, deepening as distance from shore increases. At line 93.3, this subsurface maximum persists into the fall.

## Patterns of Temporal Hydrographic Trends

Through all depths, potential density shows positive trends over time at most stations, indicating widespread isopycnal shoaling from 1988 to 2016 (Fig. 5). Shoaling is less consistent above 50 meters, with winter months being dominated by decreases in potential density. However, during this season, shoaling still appears to occur in nearshore regions. The strongest trend in density occurs at 100 meters depth.

At depths down to 50 meters, winter shows a trend of increasing temperatures; meanwhile, the remaining seasons show negative temperature trends (Fig. 6). Spring and summer temperatures show consistent trends at these depths, with decreasing temperatures over all but the southernmost offshore stations. For depths at or below 200 meters, temperature shows increases at most stations. In spring, below 200 meters, nearshore stations have trends approaching zero magnitude.

As densities increase in this region, temperatures shift from negative trends to positive trends (Fig. 7). On the 25.5 to 26 $kg/m^3$ isopycnals, temperatures show predominantly negative trends throughout the study area; however, some stations, particularly nearshore during the fall, deviate into weakly positive trends. At the 26.25 $kg/m^3$ isopyncal, a trend towards predominant warming within the system occurs, starting

nearshore. Where potential densities are greater than or equal to 26.5 kg/m$^3$, temperature increases are seen throughout the study range.

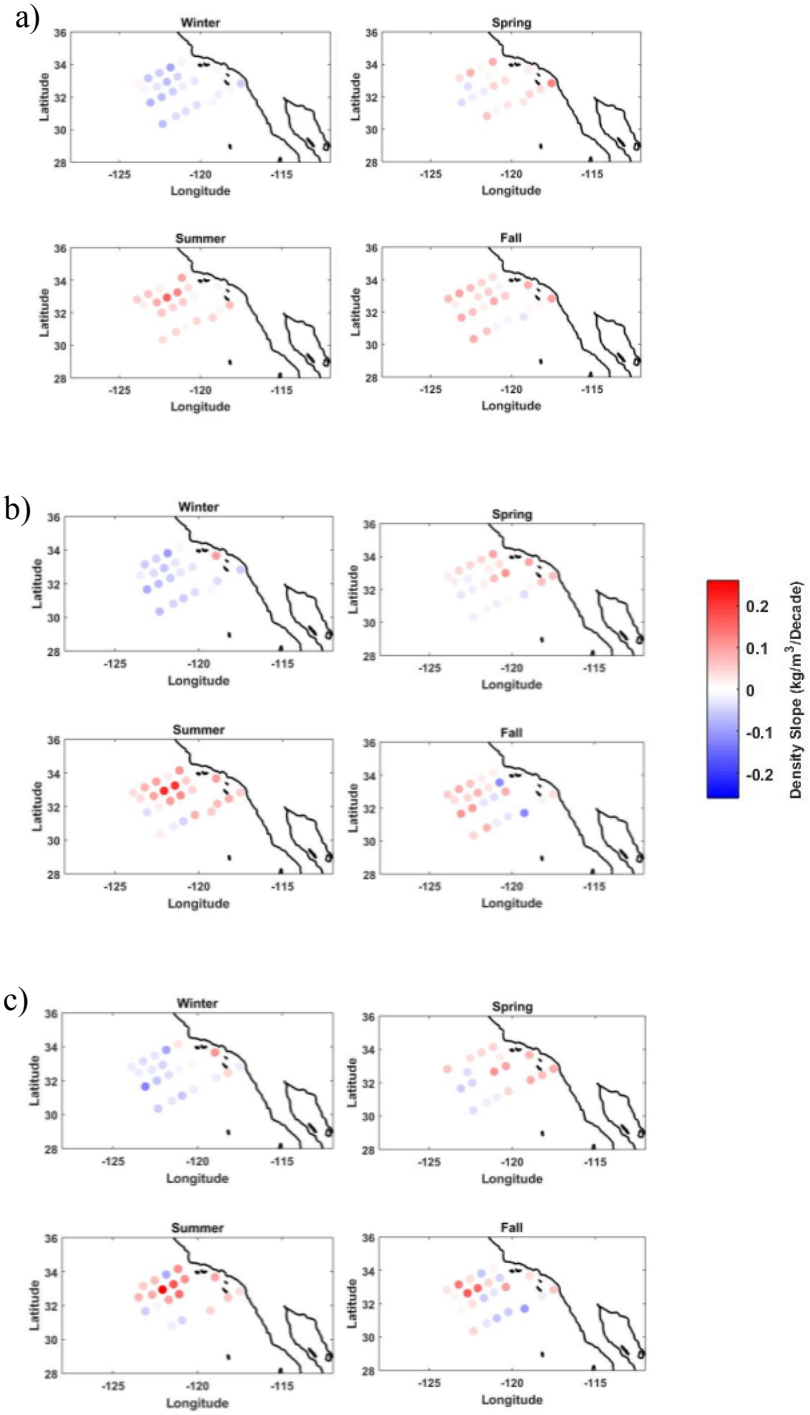

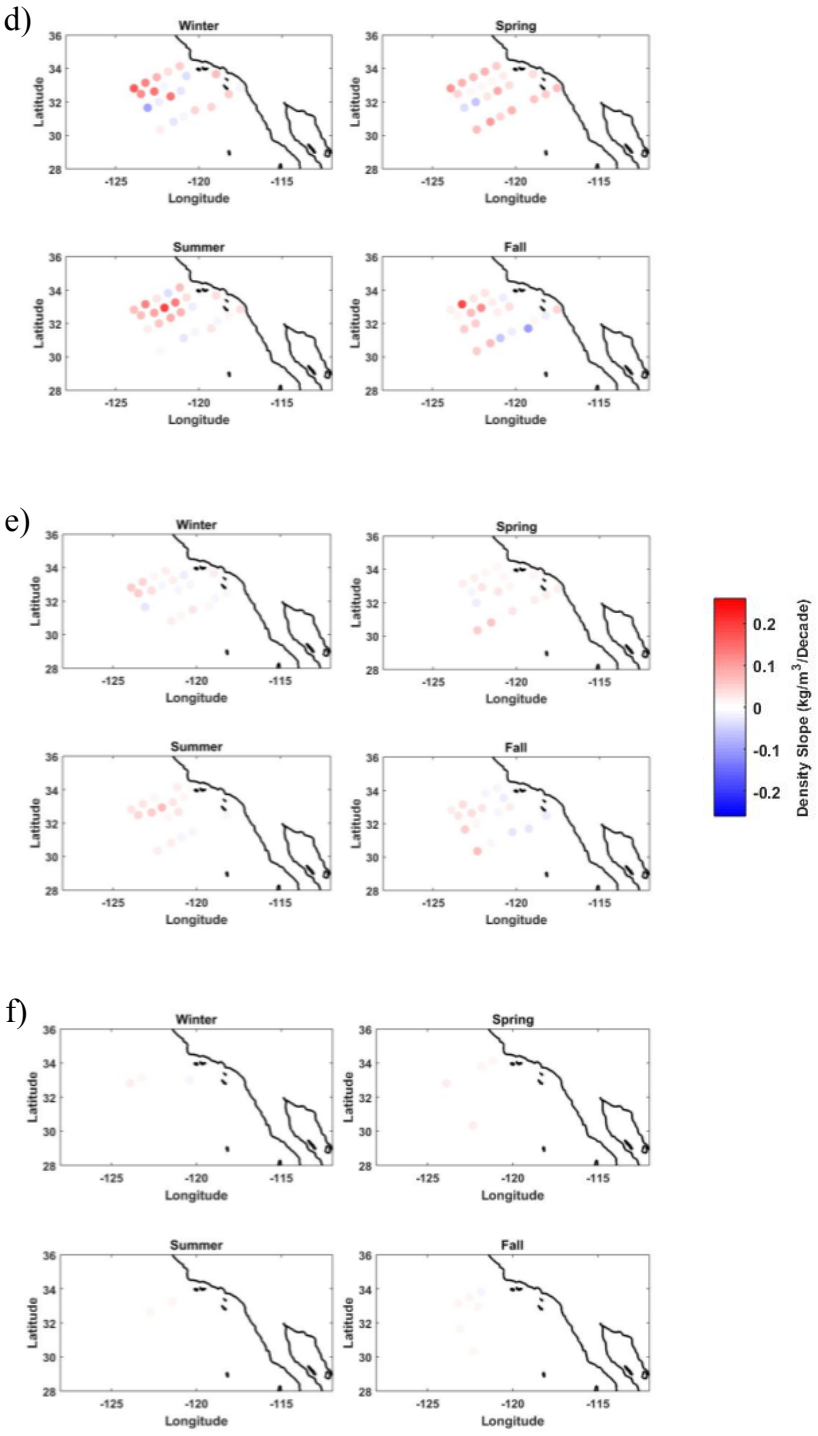


**Figure 5.** Seasonal trends of potential density at standard depths of a) 10 meters, b) 30 meters, c) 50 meters, d) 100 meters, e) 200 meters, and f) 500 meters. Trends are calculated using the non-parametric Sen's Slope over the time period from 1988 to 2016.

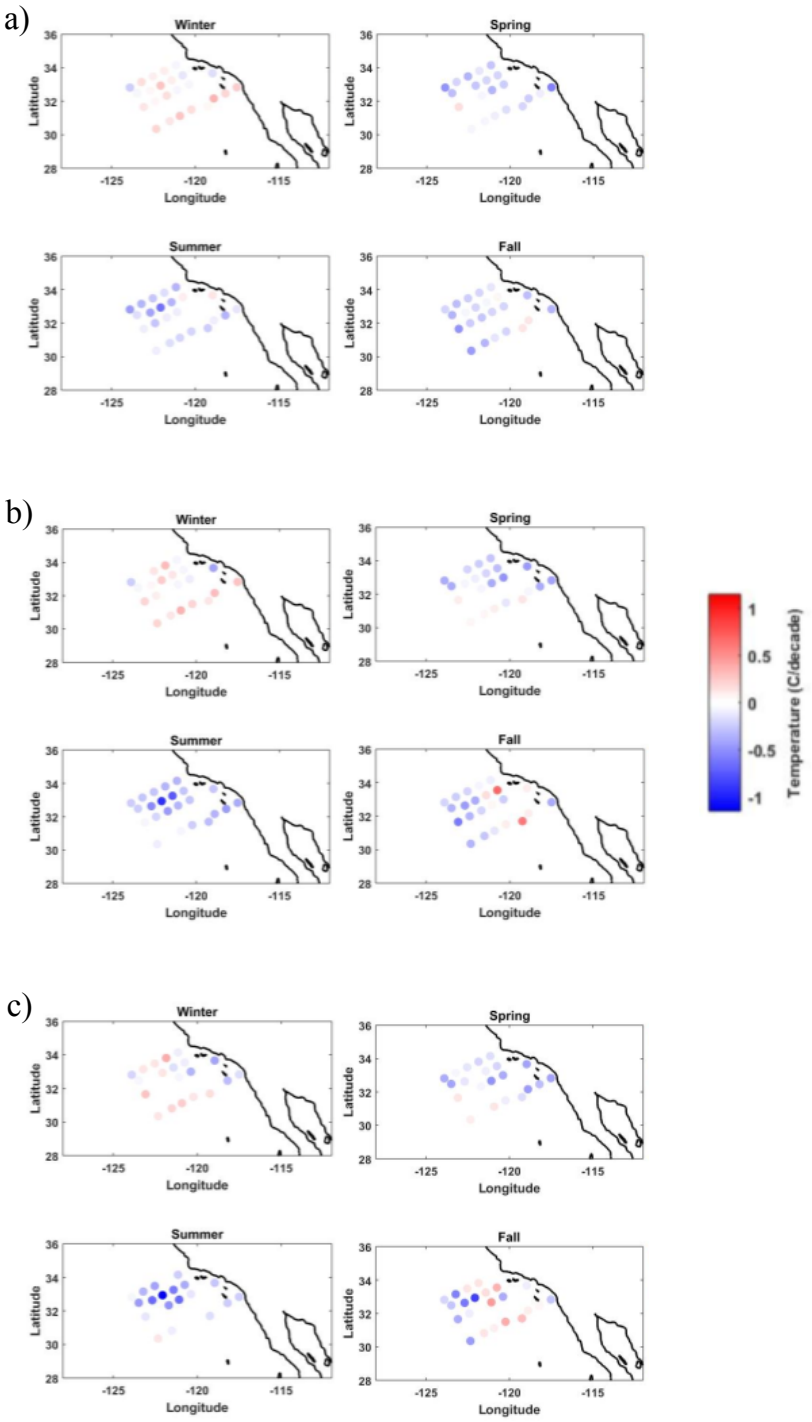
a)
Winter
Spring
Summer
Fall
b)
Winter
Spring
Summer
Fall
c)
Winter
Spring
Summer
Fall
Latitude
Longitude
36
34
32
30
28
-125
-120
-115
1
0.5
0
-0.5
-1
Temperature (C/decade)

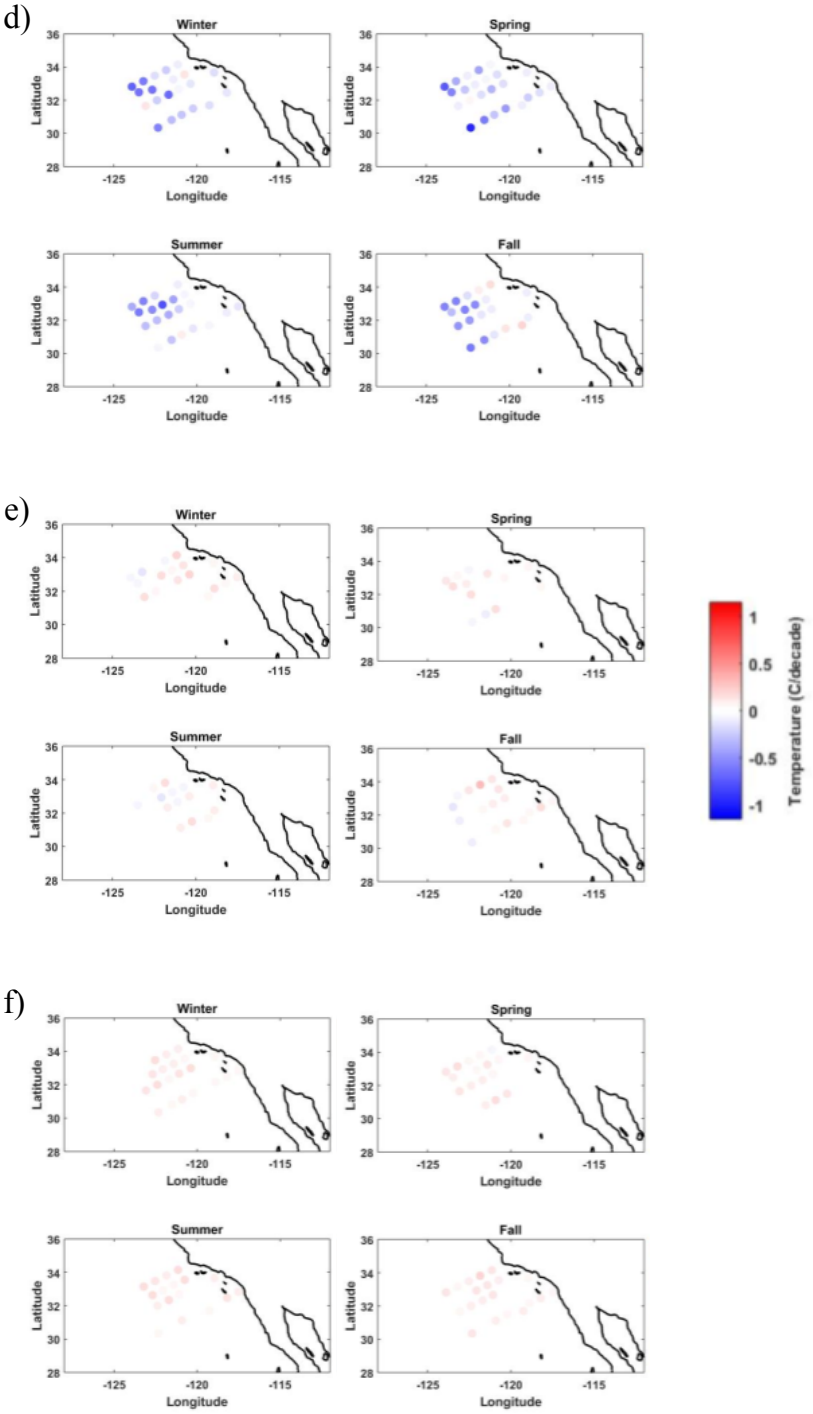


**Figure 6.** Seasonal trends of temperature at standard depths of a) 10 meters, b) 30 meters, c) 50 meters, d) 100 meters, e) 200 meters, and f) 500 meters. Trends are calculated using the non-parametric Sen's Slope over the time period from 1988 to 2016.

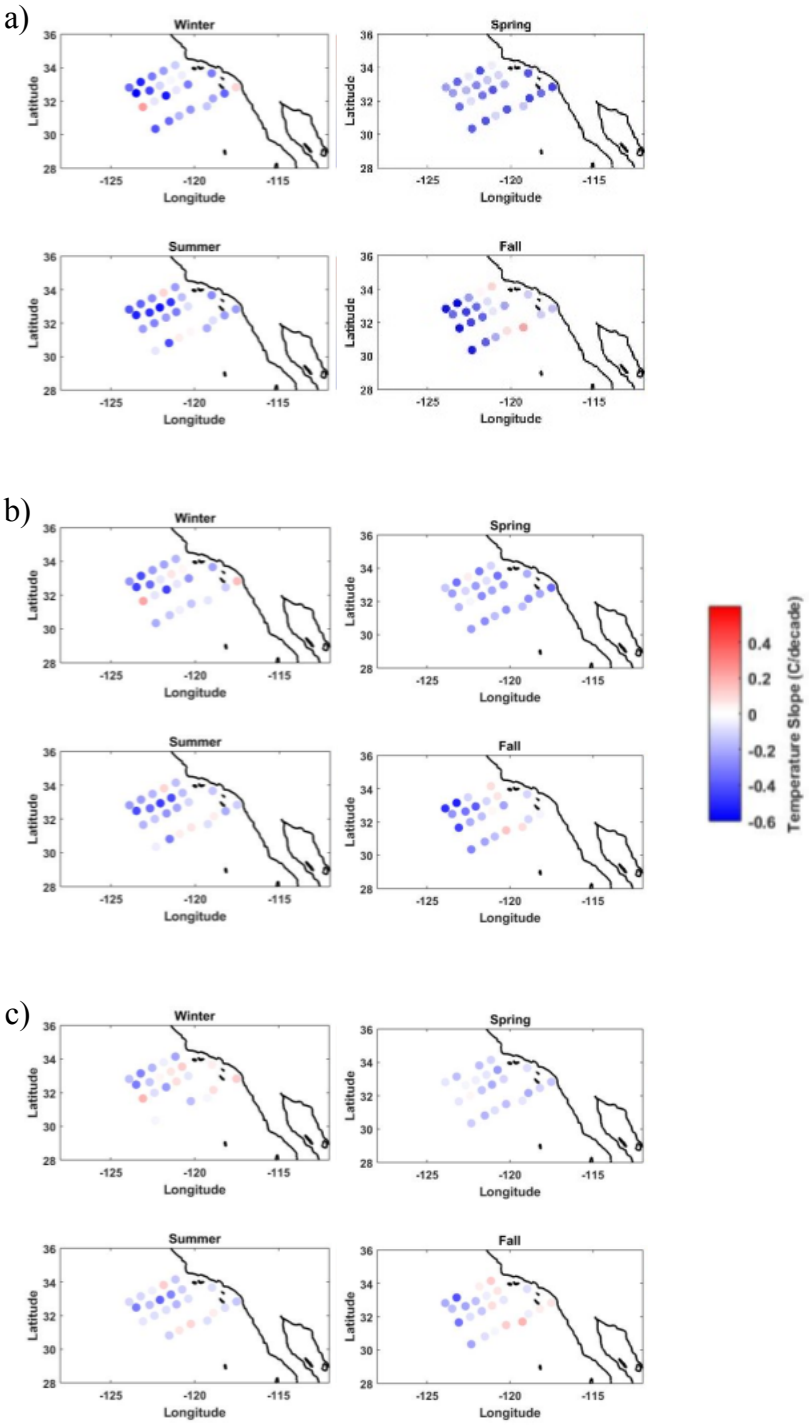
a)
Winter
Spring
Summer
Fall
b)
Winter
Spring
Summer
Fall
c)
Winter
Spring
Summer
Fall
Latitude
Longitude
36
34
32
30
28
-125
-120
-115
0.4
0.2
0
-0.2
-0.4
-0.6
Temperature Slope (C/decade)

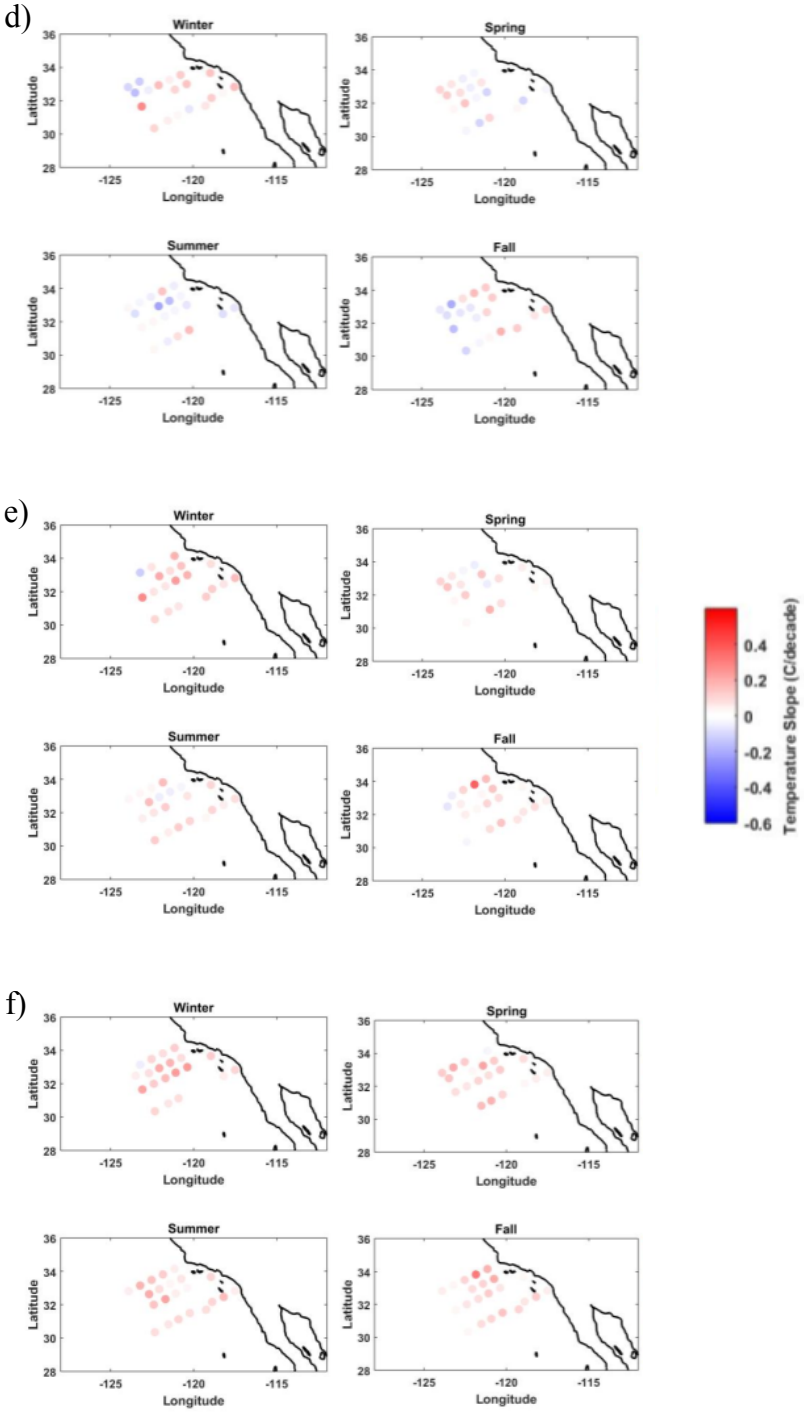


**Figure 7.** Seasonal trends of temperatures along isopycnals of a) 25.5, b) 25.75, c) 26, d) 26.25, e) 26.5, and f) 26.75 kg/m$^3$. Trends are calculated using the non-parametric Sen's Slope over the time period from 1988 to 2016.

Above 200 meters, nearshore regions display increasing salinities, while offshore regions display decreasing salinities (Fig. 8). During summer and winter, southern latitudes show more salinity increases offshore in upper waters (depth ≤ 30 m) than do northern latitudes; however, in fall, northern latitudes have more offshore salinity increases. At and below 200 meters, the study region displays primarily positive salinity trends. At depths of 500 meters, waters in and around the Bight display little salinity change.

As expected from temperature patterns, on isopycnals, salinities show the greatest decreases near the surface and increase as density increases (Fig. 9). At the 25.5 $kg/m^3$ isopycnal, salinities decrease over most of the area. There are a few scattered positive trends in most seasons, but these concentrate in northern latitudes during summer. At the 25.75 $kg/m^3$ and 26 $kg/m^3$ isopycnals, summer, fall, and winter seasons show positive salinity trends in the northern lines, decreasing in magnitude or becoming negative in the southern lines. At and below the 26 $kg/m^3$ isopycnal, positive salinity trends occur across the entire study area. The transition between positive and negative trends occurs at lower densities for salinity than for temperature (25.75 $kg/m^3$ versus 26 $kg/m^3$), potentially as a result of limited resolution involved with the linear interpolation of variables to isopycnals.

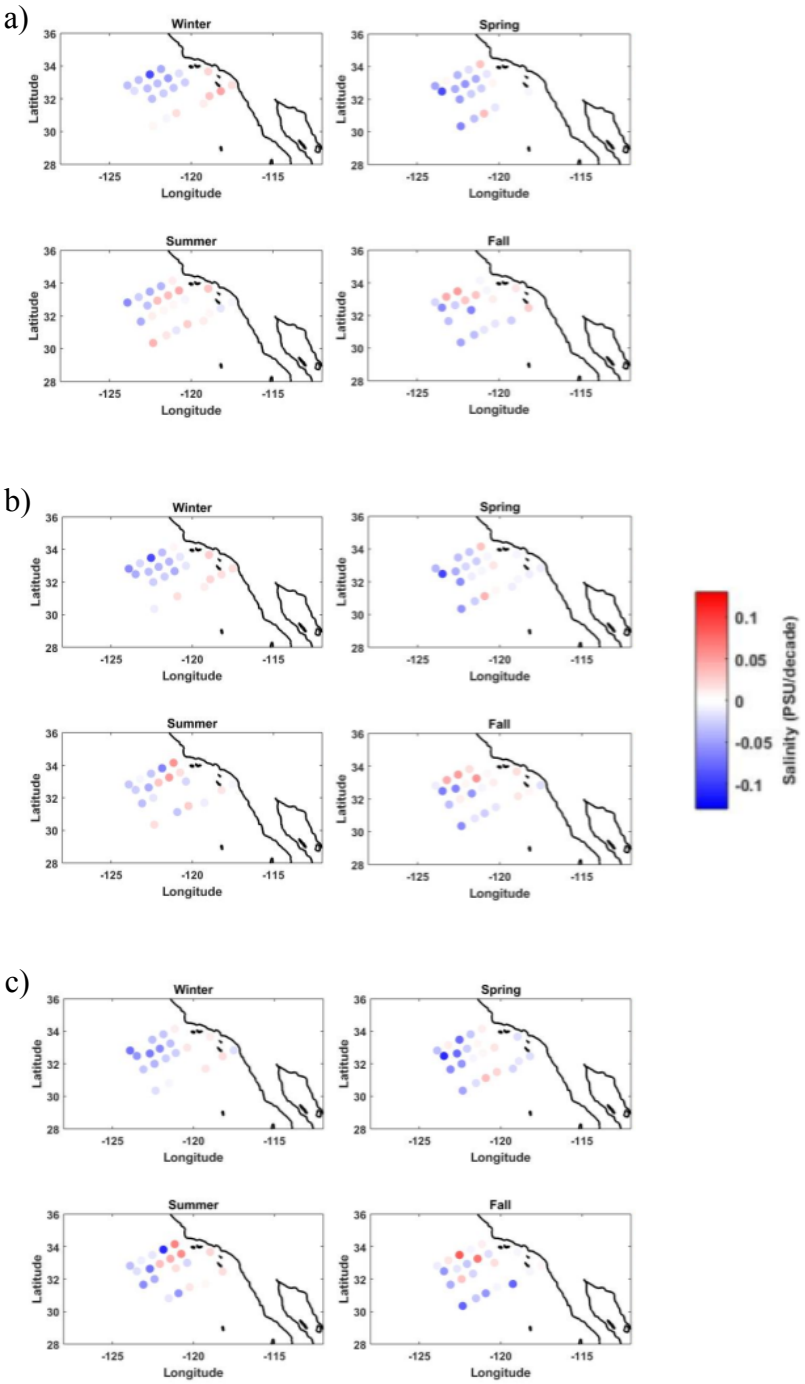
a)
Winter
Spring
Summer
Fall
b)
Winter
Spring
Summer
Fall
c)
Winter
Spring
Summer
Fall
Latitude
Longitude
36
34
32
30
28
-125
-120
-115
0.1
0.05
0
-0.05
-0.1
Salinity (PSU/decade)

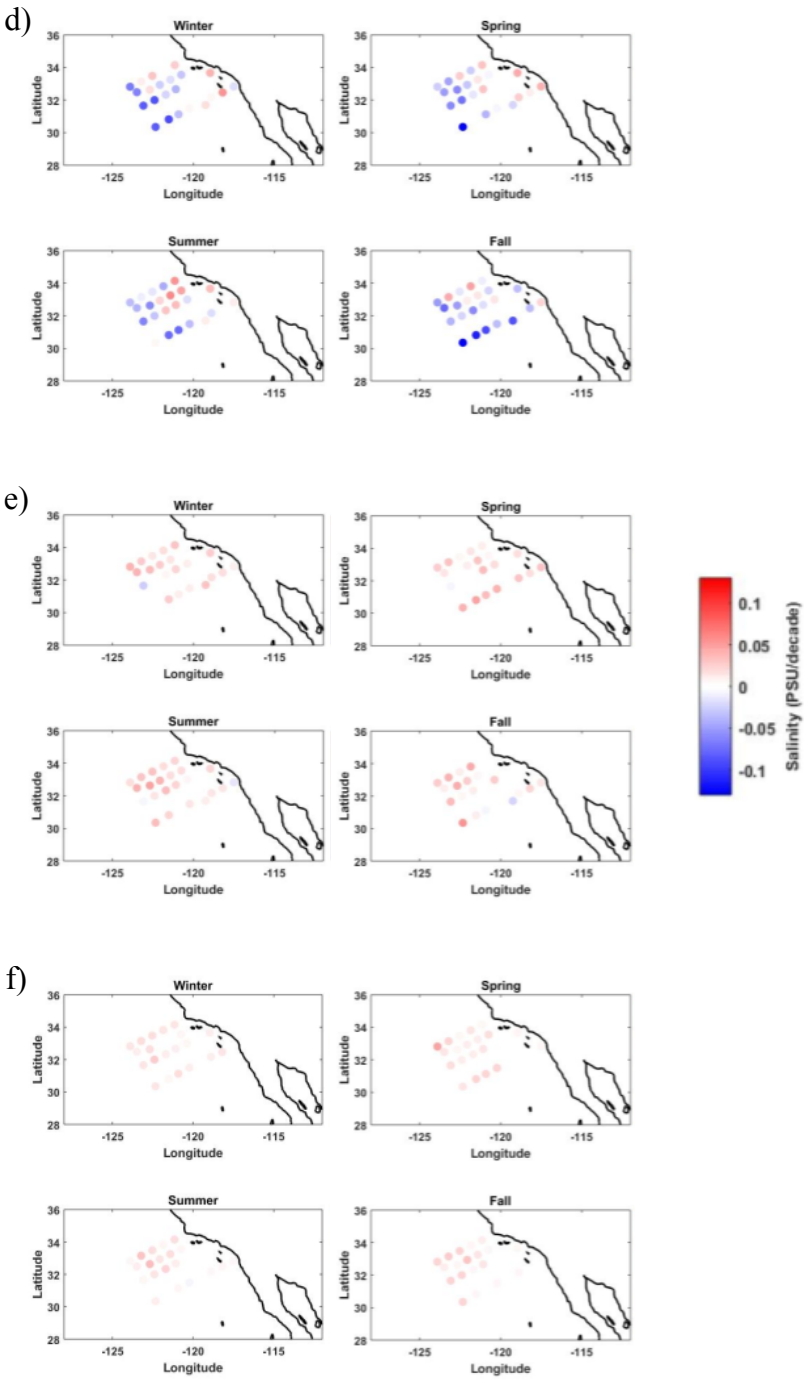


**Figure 8.** Seasonal trends of salinities at standard depths of a) 10 meters, b) 30 meters, c) 50 meters, d) 100 meters, e) 200 meters, and f) 500 meters. Trends are calculated using the non-parametric Sen's Slope over the time period from 1988 to 2016.

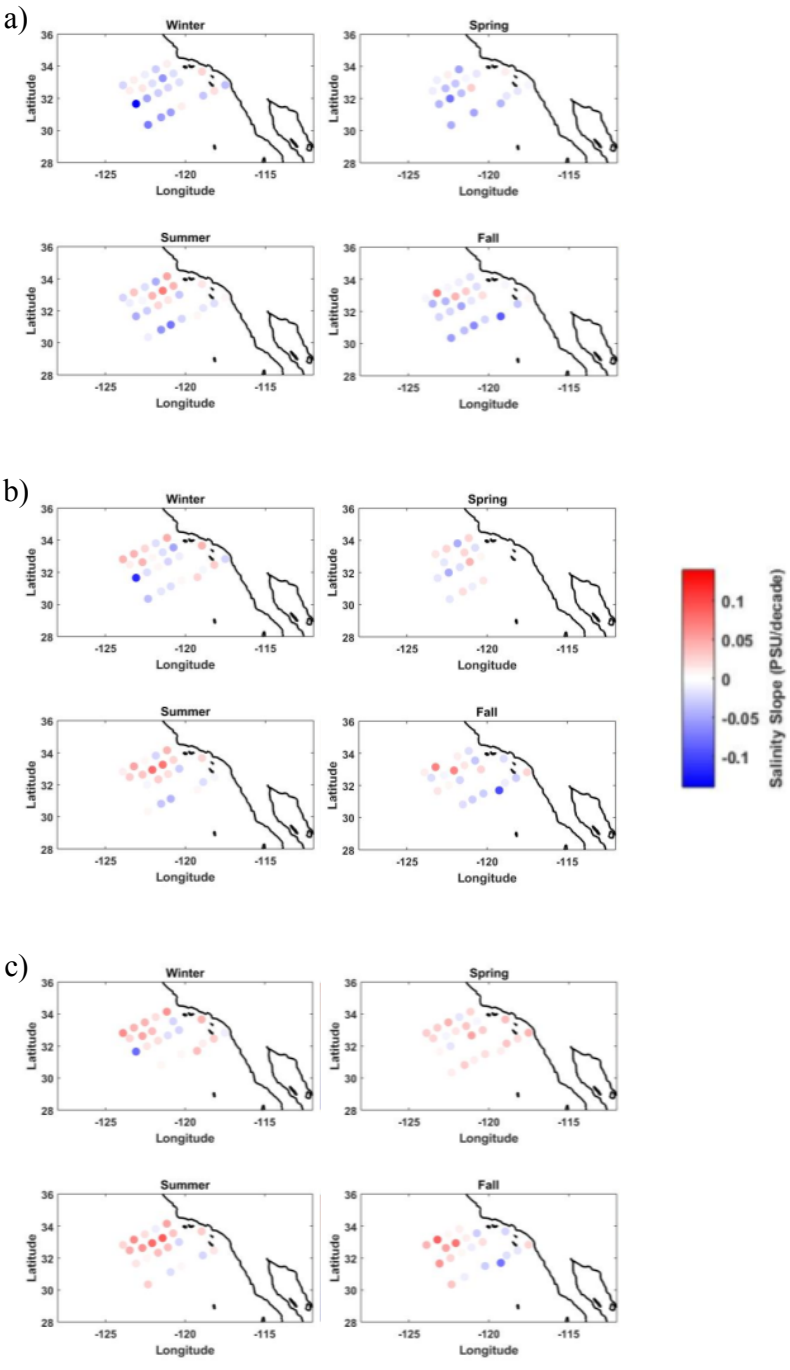
a)
b)
c)
Winter
Spring
Summer
Fall
Latitude
Longitude
36
34
32
30
28
-125
-120
-115
0.1
0.05
0
-0.05
-0.1
Salinity Slope (PSU/decade)

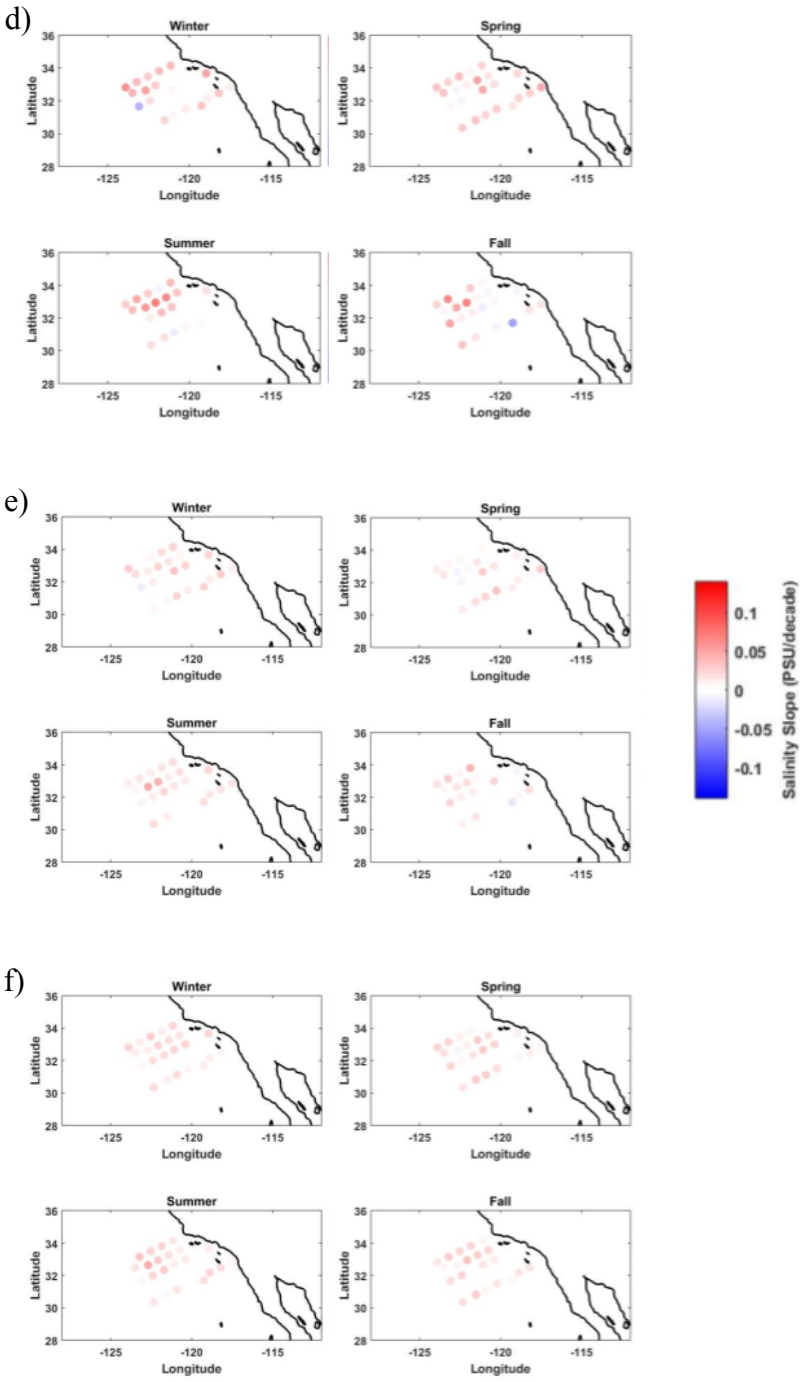


**Figure 9.** Seasonal trends of salinities along isopycnals of a) 25.5, b) 25.75, c) 26, d) 26.25, e) 26.5, and f) 26.75 kg/m$^3$. Trends are calculated using the non-parametric Sen's Slope over the time period from 1988 to 2016.

## Patterns of Temporal Oxygen Trends

Maximum deoxygenation trends, approaching 0.5 ml/L/decade, occur at depths of 200 meters, spread over the whole study area (Fig. 10). Moving away from 200 meters, deoxygenation trends weaken. At offshore stations, oxygen concentrations quickly become characterized by a lack of evident trends. However, at depths of 30 to 50 meters, nearshore stations maintain higher deoxygenation rates than do offshore stations, especially in winter and summer. At depths of 10 meters or 500 meters, trends in oxygen concentration become minimal. While oxygen concentrations at 500 meters are characterized by consistent, weak deoxygenation, oxygen concentrations at 10 meters are characterized by seasonal variability in weak positive and negative trends.

With few exceptions, stations display deoxygenation along isopycnals (Fig. 11). Along isopycnals of potential densities 25.5 and 25.75 $kg/m^3$, oxygen concentrations show elevated rates of decrease along lines 80 and 83.3 compared to lines 86.7 and 93.3 during winter, summer, and fall. This trend occurs in winter and summer at potential densities of 26 $kg/m^3$, as well. Additionally, the 26 $kg/m^3$ isopycnal displays greater deoxygenation nearshore in the spring and offshore in the fall. At 26.25 $kg/m^3$, summer and fall months display increased deoxygenation offshore relative to nearshore within the Southern California Bight. During winter and spring, deoxygenation rates show an even cross-shore distribution along the Bight. Deoxygenation rates peak along the 26.5 $kg/m^3$ isopycnal, once again approaching rates of 0.5 ml/L/decade.

As a final note on temporal trends, strong interannual variability occurs across all lines and all seasons within the study period (Fig. 12-15). Between isopycnals at each station, the pattern of variability (i.e.- temporal occurrence of positive or negative

anomalies) remains stable. However, with increasing density, these anomalies show decreasing magnitude.

With the above trends in mind, the Sen's slope formulations for oxygen concentration shown throughout the study largely showed low significance, often with $p > 0.20$. However, with increasing depth (density) significance increased, occasionally showing strong relationships with $p < 0.10$. Temperature and salinity did not show this significance increase with depth. While significance in general proved low, calculated trends for individual variables tended to remain spatially consistent (Fig. 5-11).

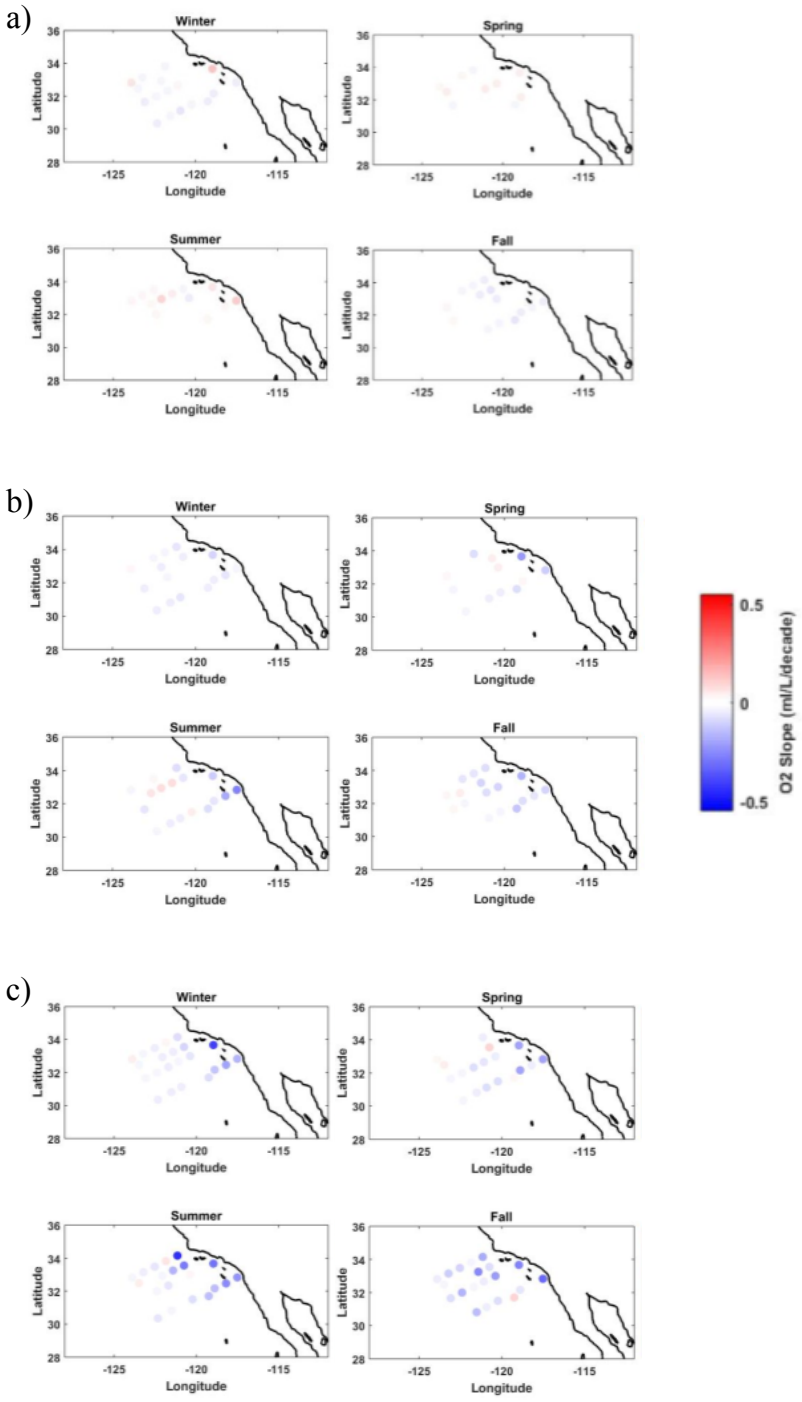
a)
Winter
Spring
Summer
Fall
b)
Winter
Spring
Summer
Fall
c)
Winter
Spring
Summer
Fall
Latitude
Longitude
36
34
32
30
28
-125
-120
-115
0.5
0
-0.5
O2 Slope (ml/L/decade)

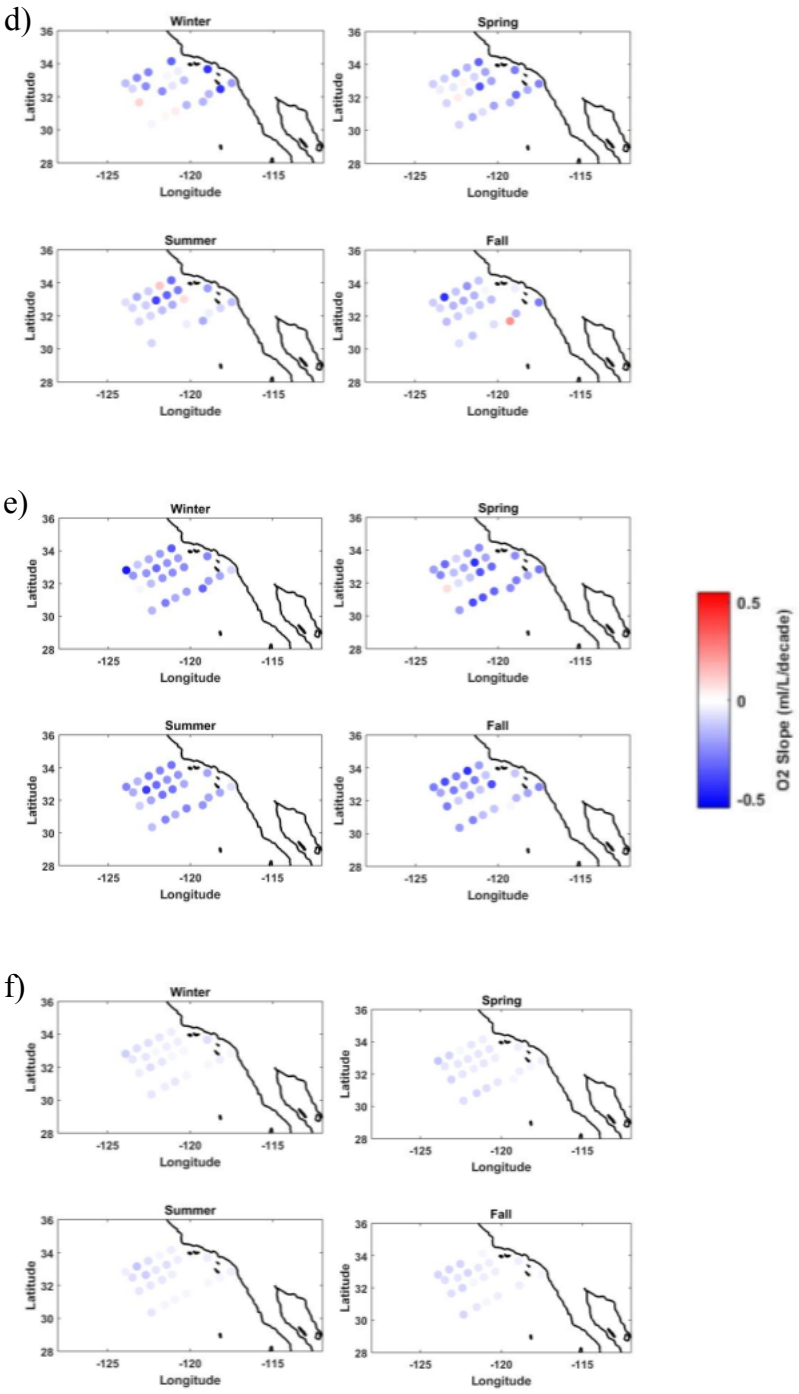


**Figure 10.** Seasonal trends of oxygen concentrations at standard depths of a) 10 meters, b) 30 meters, c) 50 meters, d) 100 meters, e) 200 meters, and f) 500 meters. Trends are calculated using the non-parametric Sen's Slope over the time period from 1988 to 2016.

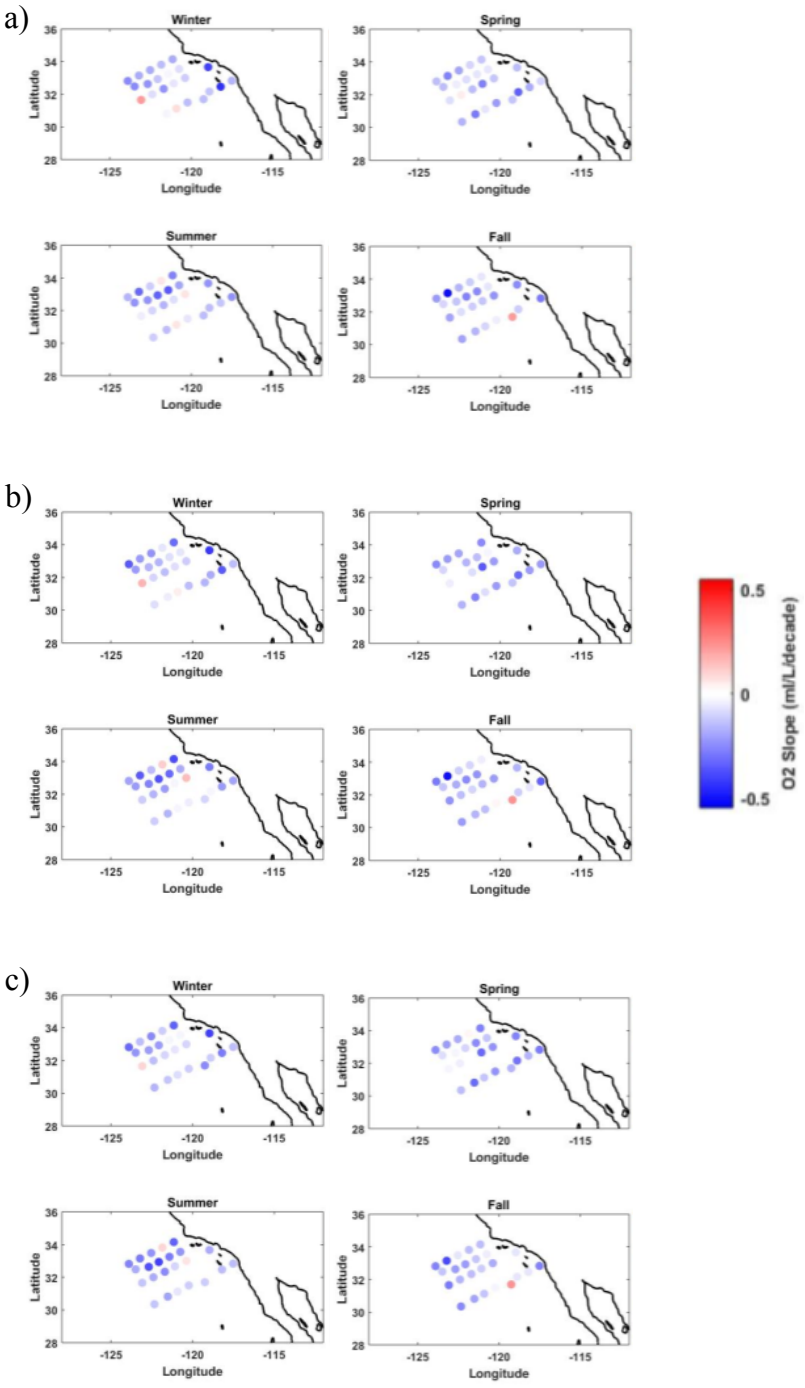
a)
Winter
Spring
Summer
Fall
b)
Winter
Spring
Summer
Fall
c)
Winter
Spring
Summer
Fall
Latitude
Longitude
36
34
32
30
28
-125
-120
-115
0.5
0
-0.5
O2 Slope (ml/L/decade)

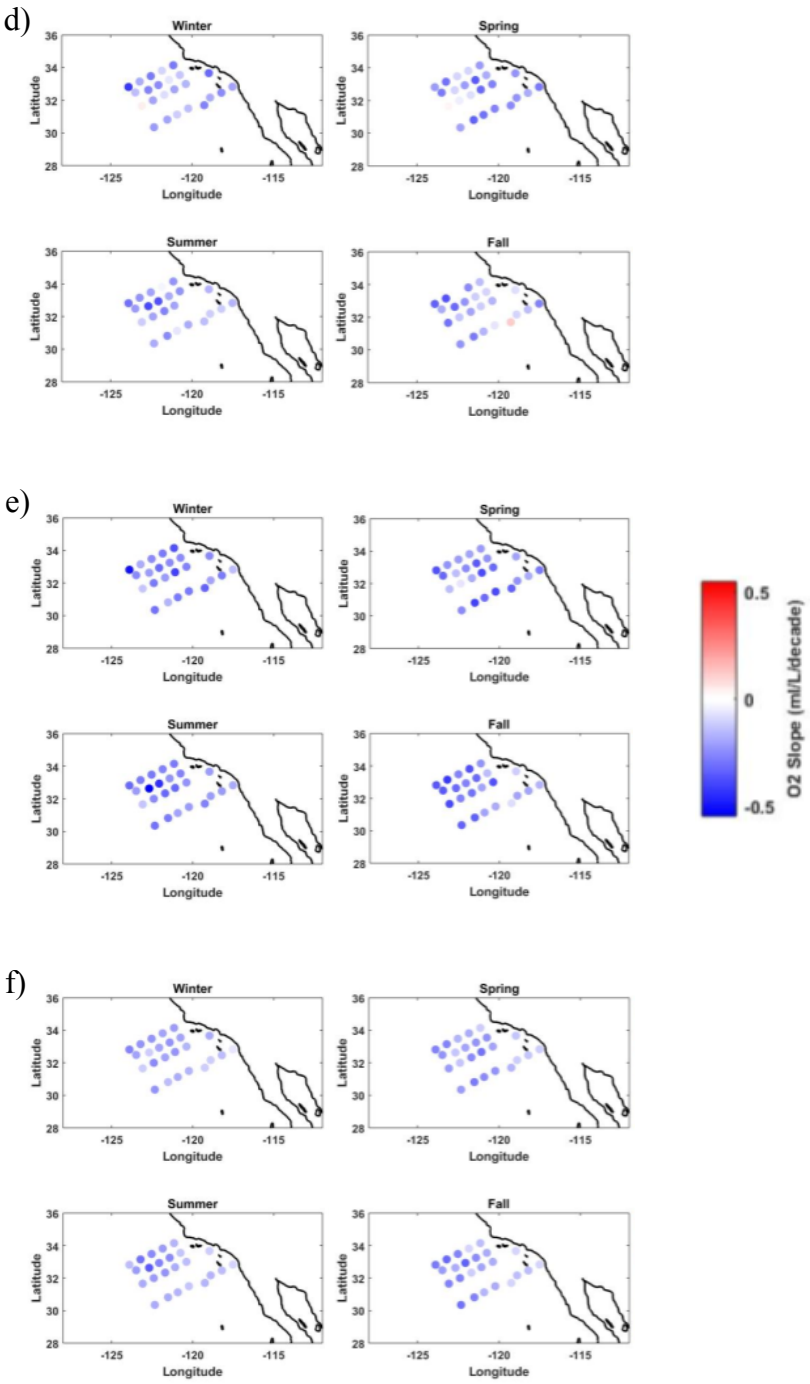


**Figure 11.** Seasonal trends of oxygen concentrations along isopycnals of a) 25.5, b) 25.75, c) 26, d) 26.25, e) 26.5, and f) 26.75 kg/m$^3$. Trends are calculated using the non-parametric Sen's Slope over the time period from 1988 to 2016.

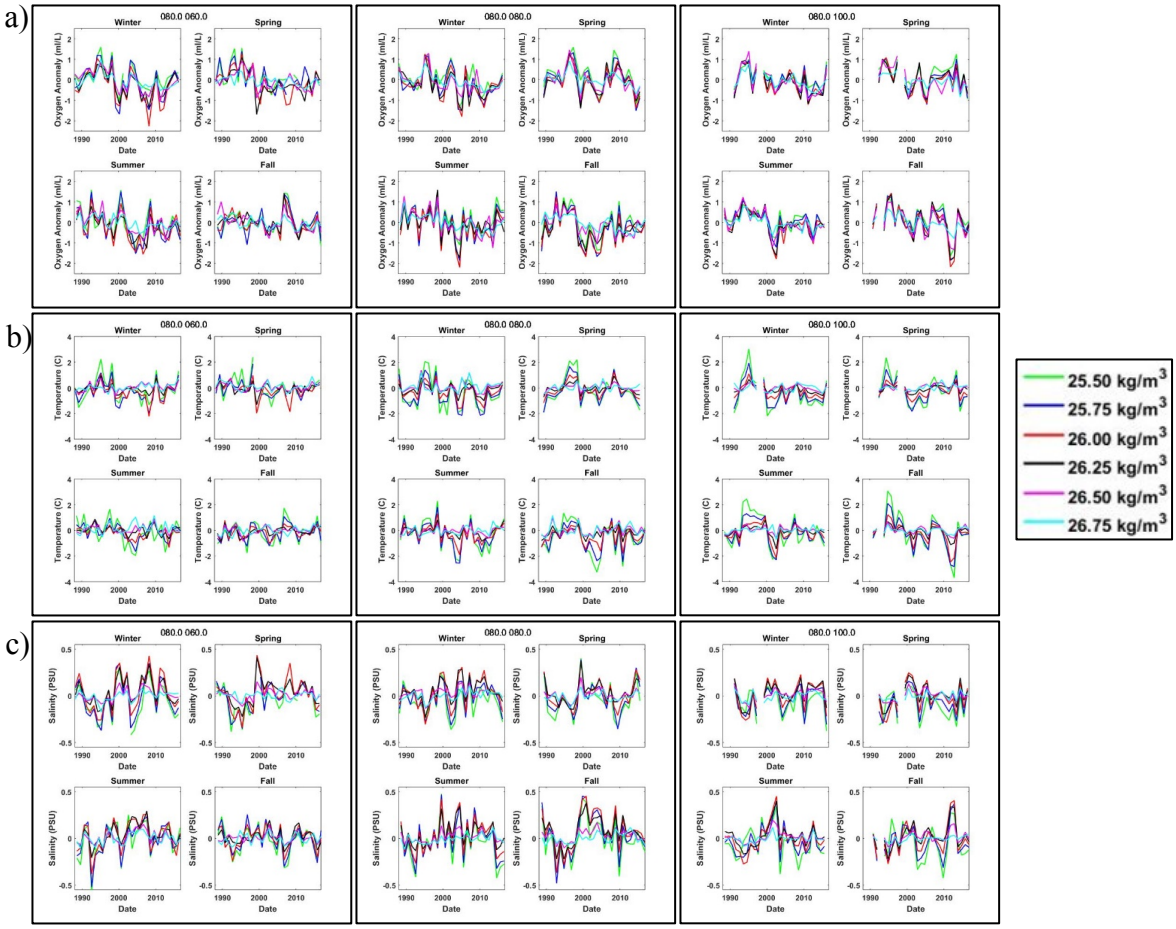


**Figure 12.** Time series of seasonal a) oxygen concentration anomalies, b) temperature anomalies, and c) salinity anomalies along isopycnals over the period of 1988 to 2016 at three stations on line 80. Isopycnal values represent potential densities. Anomalies are calculated against seasonal mean values from 1950 to 2016. From left to right, the stations are 80 60, 80 80, and 80 100. Stations move cross-shelf away from shore, with station 80 60 representing the nearest station to shore utilized in this study.

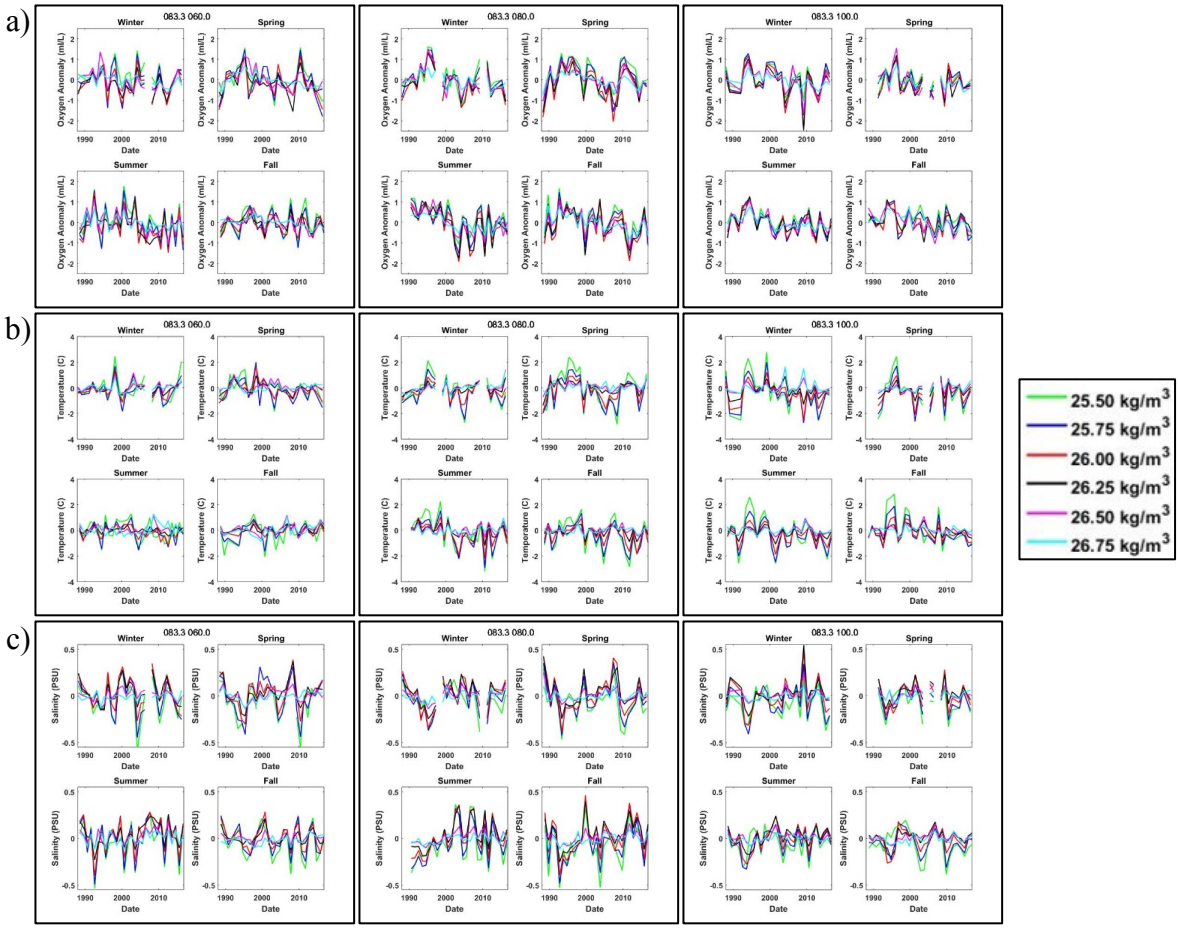


**Figure 13.** Time series of seasonal a) oxygen concentration anomalies, b) temperature anomalies, and c) salinity anomalies along isopycnals over the period of 1988 to 2016 at three stations on line 83.3. Isopycnal values represent potential densities. Anomalies are calculated against seasonal mean values from 1950 to 2016. From left to right, the stations are 83.3 60, 83.3 80, and 83.3 100. Stations move cross-shelf away from shore, with station 83.3 60 representing the nearest station to shore utilized in this study.

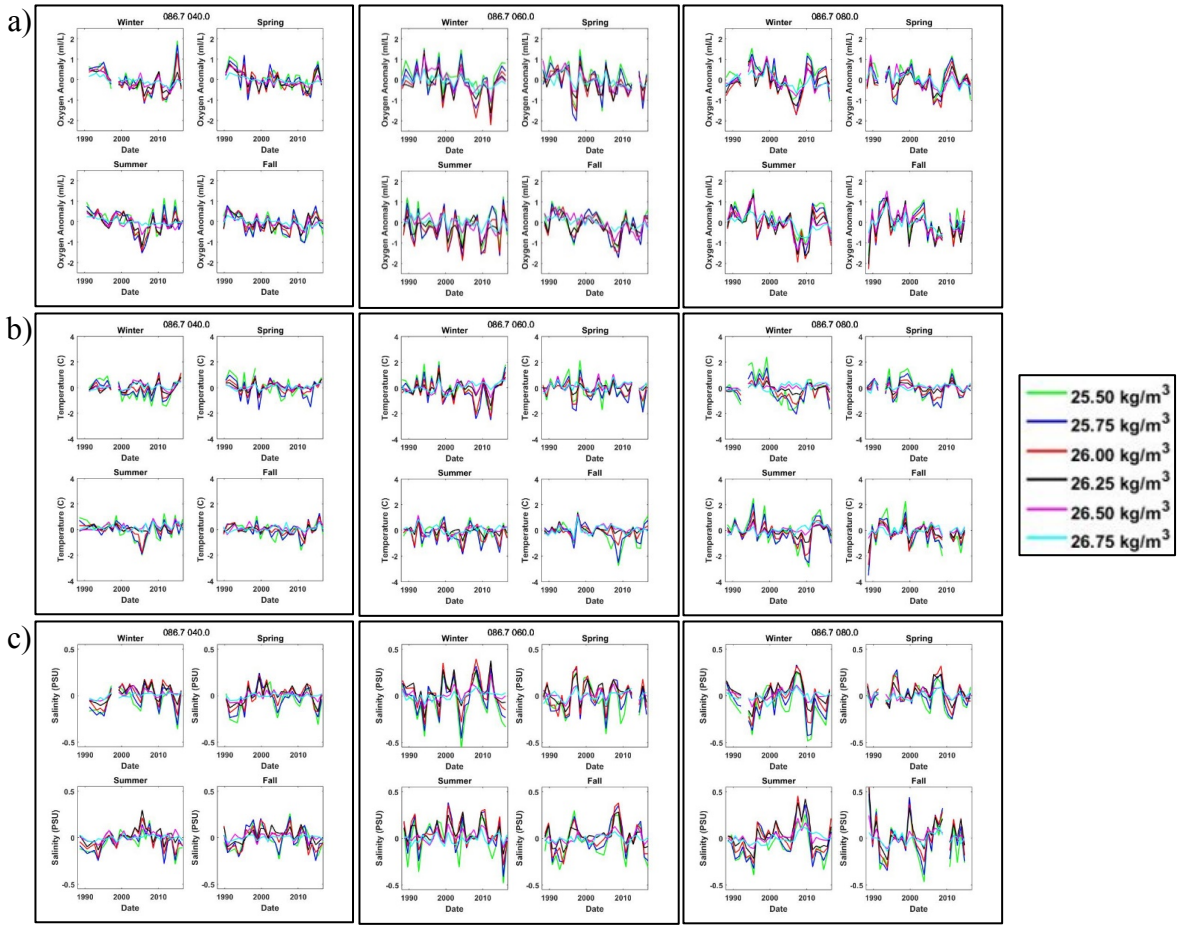


**Figure 14.** Time series of seasonal a) oxygen concentration anomalies, b) temperature anomalies, and c) salinity anomalies along isopycnals over the period of 1988 to 2016 at three stations on line 86.7. Isopycnal values represent potential densities. Anomalies are calculated against seasonal mean values from 1950 to 2016. From left to right, the stations are 86.7 40, 86.7 60, and 86.7 80. Stations move cross-shelf away from shore, with station 086.7 040.0 representing the nearest station to shore utilized in this study.

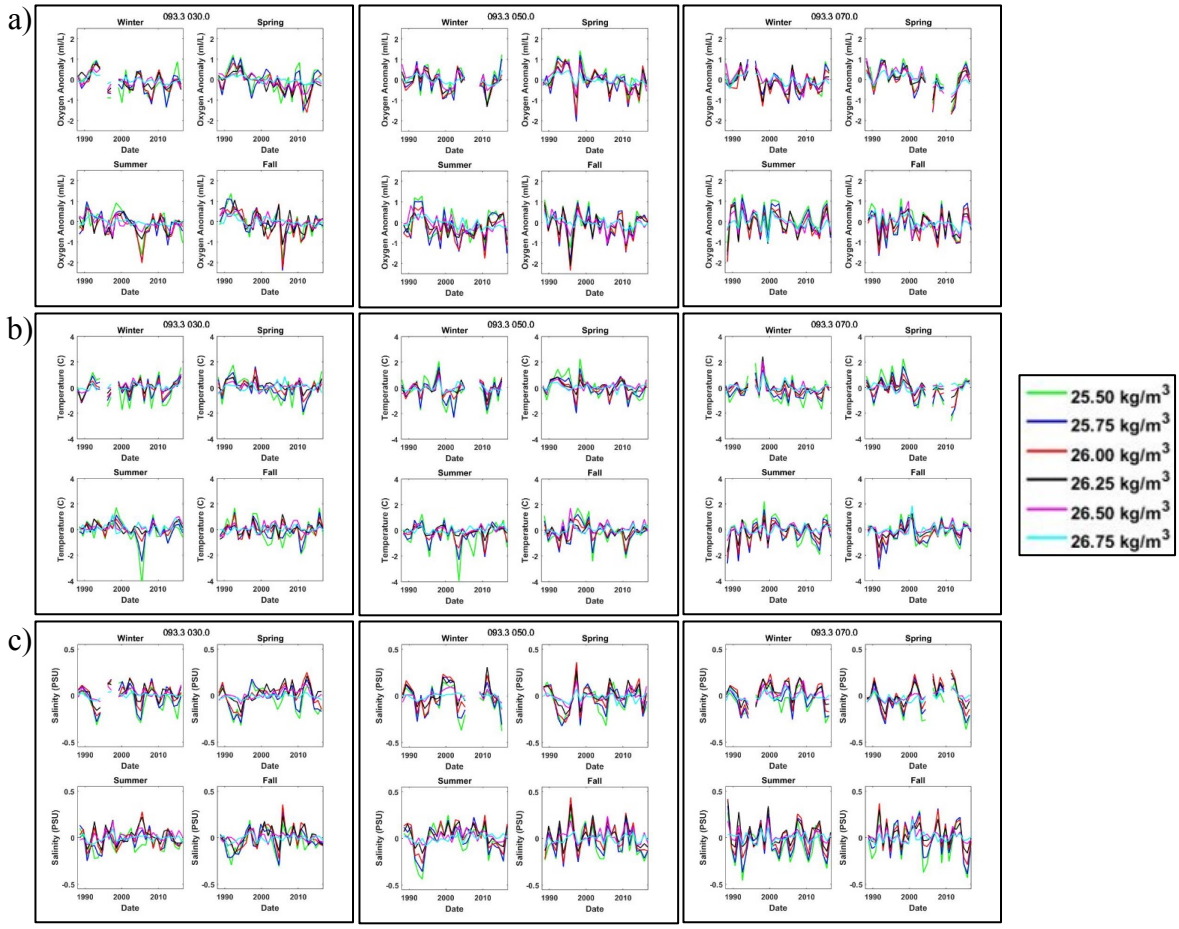


**Figure 15.** Time series of seasonal a) oxygen concentration anomalies, b) temperature anomalies, and c) salinity anomalies along isopycnals over the period of 1988 to 2016 at three stations on line 93.3. Isopycnal values represent potential densities. Anomalies are calculated against seasonal mean values from 1950 to 2016. From left to right, the stations are 93.3 30, 093.3 50, and 93.3 70. Stations move cross-shelf away from shore, with station 93.3 30 representing the nearest station to shore utilized in this study.

Comparison of Oxygen Concentration Trends to Hydrographic Properties

Oxygen trends show no strong correlation with temperature trends when viewed at equal depths (Fig. 16). Although correlation increases near the surface, $R^2$ values reach 0.5 only once (Fig. 16a). Correlation between oxygen trends and salinity trends increase with depth, reaching $R^2$ values above 0.8 at 500 meters and generally showing $R^2$ values above 0.5 at and below 100 meters (Fig. 17).

When viewed on isopycnals, correlation between oxygen trends and temperature trends remain low (Fig. 18). However, an increase in correlation is seen at potential densities less than 26.0 kg/m$^3$ (Fig. 18a,b). Even so, correlation values rarely rise above 0.5. Oxygen trends once again show higher correlation with salinity trends (Fig. 19). At potential densities greater than or equal to 26.25 kg/m$^3$, $R^2$ values congregate around 0.6 (Fig. 19c-f). Moving up through the water column, correlation increases in strength, similar to patterns seen with temperature. Overall, as temperature trends become more positive, oxygen trends become more positive where relationships exist (Fig. 18). Conversely, as salinity trends become more negative, oxygen trends become more positive (Fig. 19).

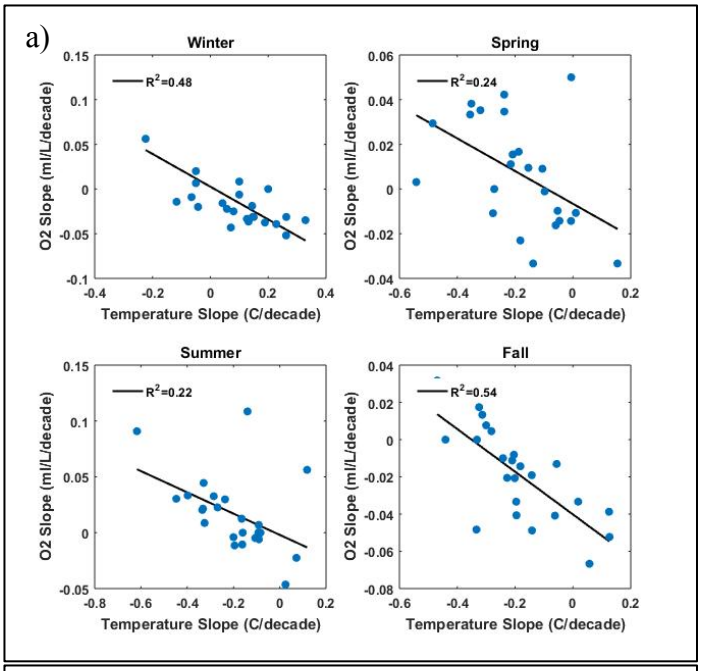
a)
Winter
R²=0.48
Spring
R²=0.24
Summer
R²=0.22
Fall
R²=0.54
O2 Slope (ml/L/decade)
Temperature Slope (C/decade)

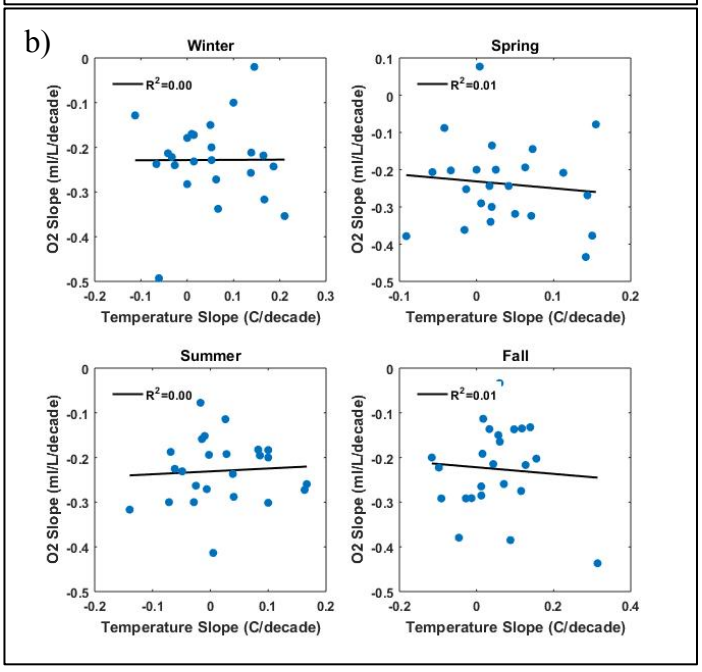
b)
Winter
R²=0.00
Spring
R²=0.01
Summer
R²=0.00
Fall
R²=0.01
O2 Slope (ml/L/decade)
Temperature Slope (C/decade)

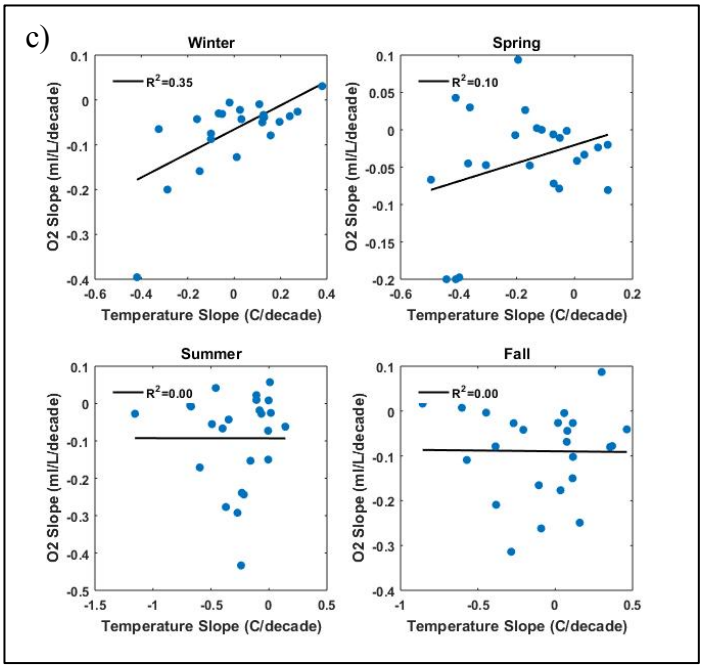
c)
Winter
R²=0.35
Spring
R²=0.10
Summer
R²=0.00
Fall
R²=0.00
O2 Slope (ml/L/decade)
Temperature Slope (C/decade)

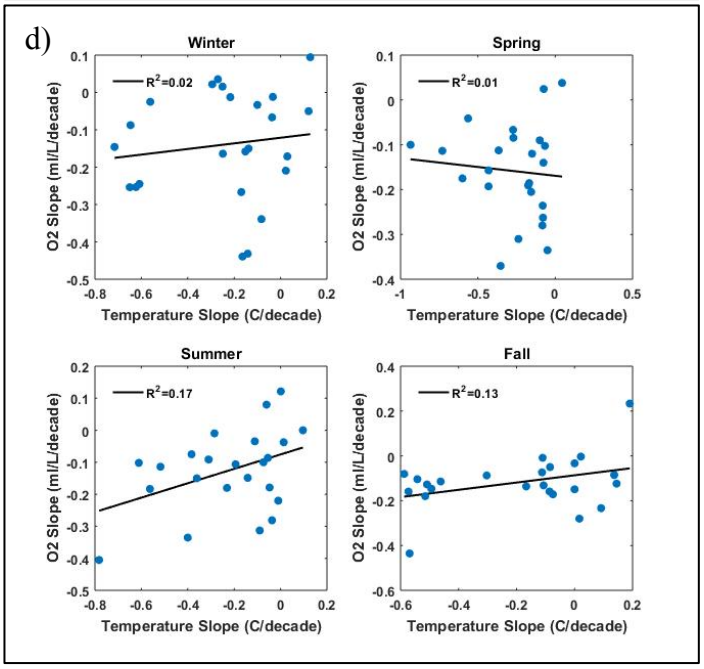
d)
Winter
R²=0.02
Spring
R²=0.01
Summer
R²=0.17
Fall
R²=0.13
O2 Slope (ml/L/decade)
Temperature Slope (C/decade)

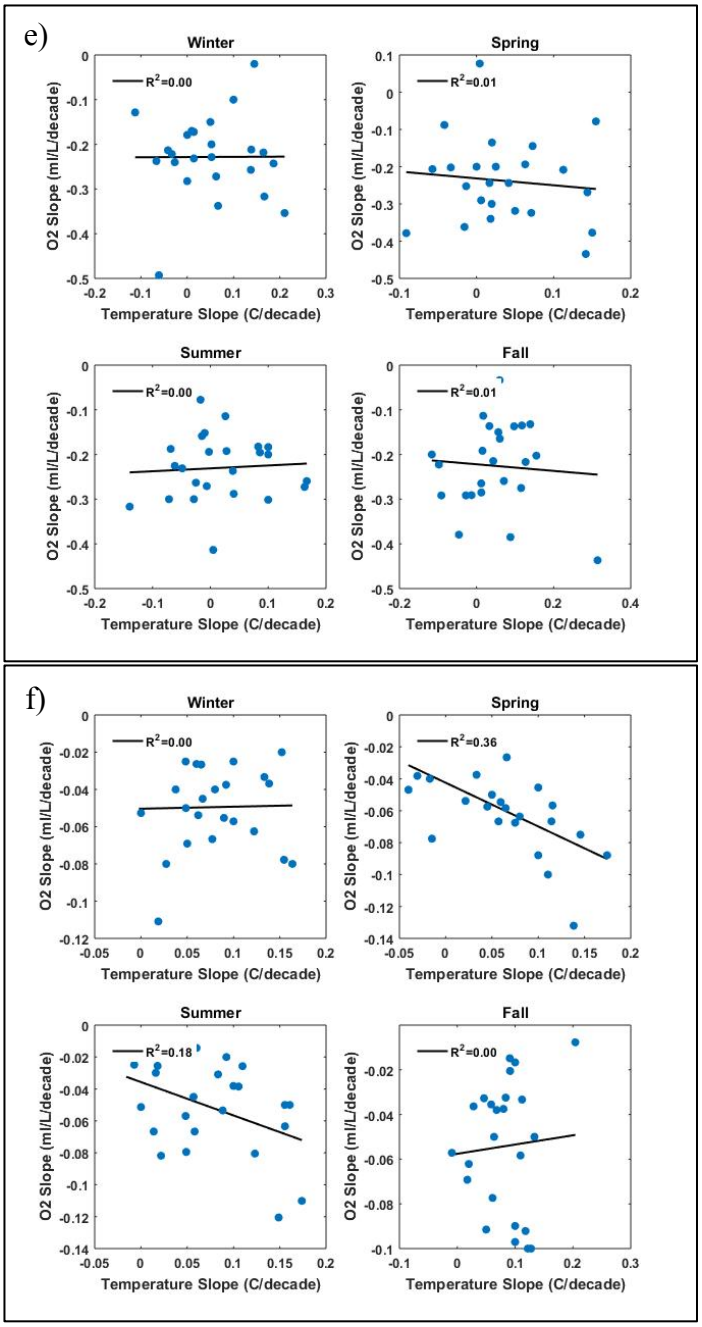


**Figure 16.** Seasonal comparison of oxygen concentration trends to temperature trends at depths of a) 10 meters, b) 30 meters, c) 50 meters, d) 100 meters, e) 200 meters, and f) 500 meters. Trends of variables are calculated using Sen's slope. Each point represents the oxygen and temperature values of an individual station at the specified depth. The black linear trend line represents a least-square regression between the two variables, and its $R^2$ value is given.

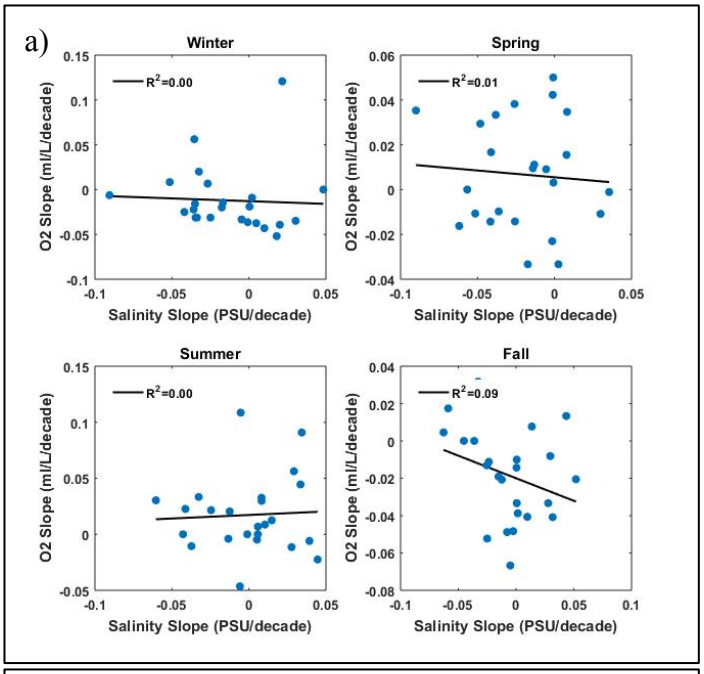
a)
Winter
R²=0.00
Spring
R²=0.01
Summer
R²=0.00
Fall
R²=0.09
O2 Slope (ml/L/decade)
Salinity Slope (PSU/decade)

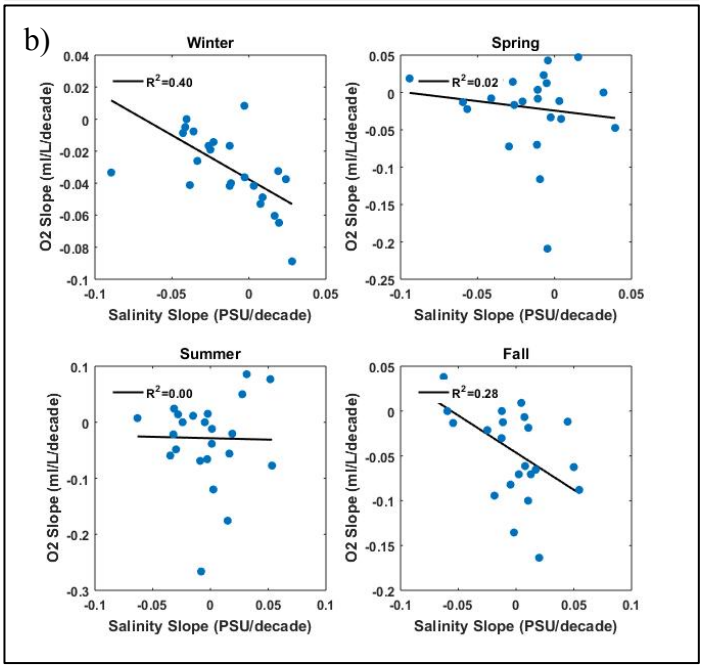
b)
Winter
R²=0.40
Spring
R²=0.02
Summer
R²=0.00
Fall
R²=0.28
O2 Slope (ml/L/decade)
Salinity Slope (PSU/decade)

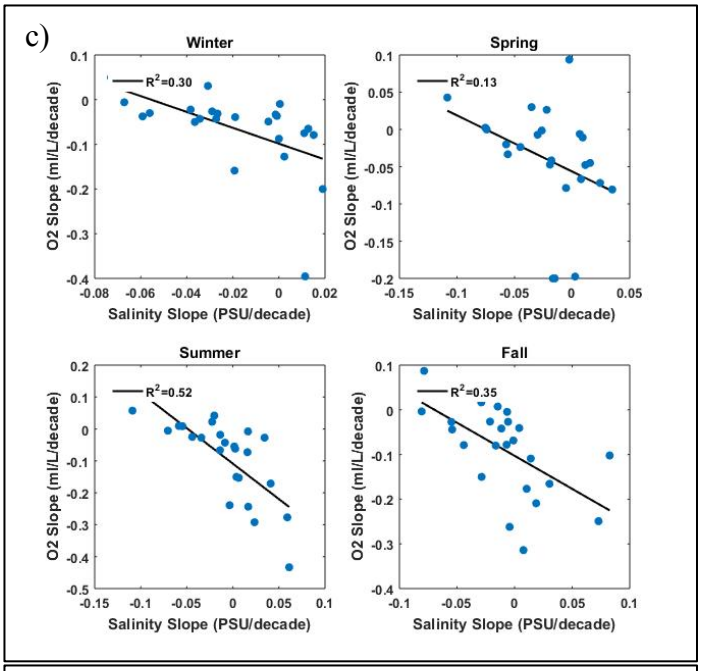
c)
Winter
R²=0.30
Spring
R²=0.13
Summer
R²=0.52
Fall
R²=0.35
O2 Slope (ml/L/decade)
Salinity Slope (PSU/decade)

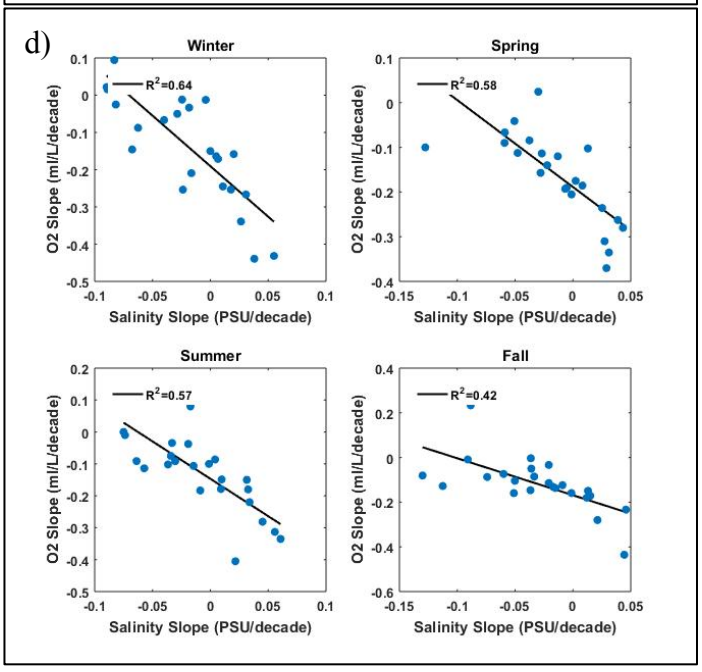
d)
Winter
R²=0.64
Spring
R²=0.58
Summer
R²=0.57
Fall
R²=0.42
O2 Slope (ml/L/decade)
Salinity Slope (PSU/decade)

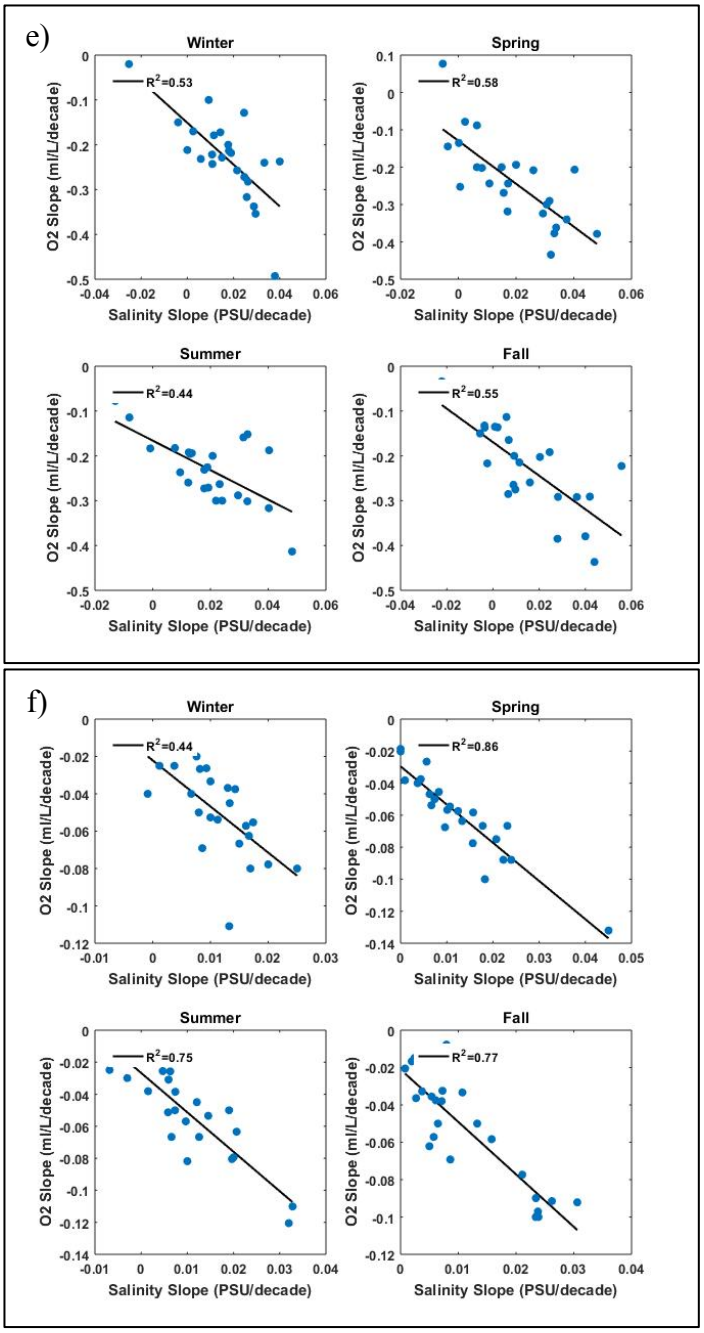


**Figure 17.** Seasonal comparison of oxygen concentration trends to salinity trends at depths of a) 10 meters, b) 30 meters, c) 50 meters, d) 100 meters, e) 200 meters, and f) 500 meters. Trends of variables are calculated using Sen's slope. Each point represents the oxygen and salinity values of an individual station at the specified depth. The black linear trend line represents a least-square regression between the two variables, and its $R^2$ value is given.

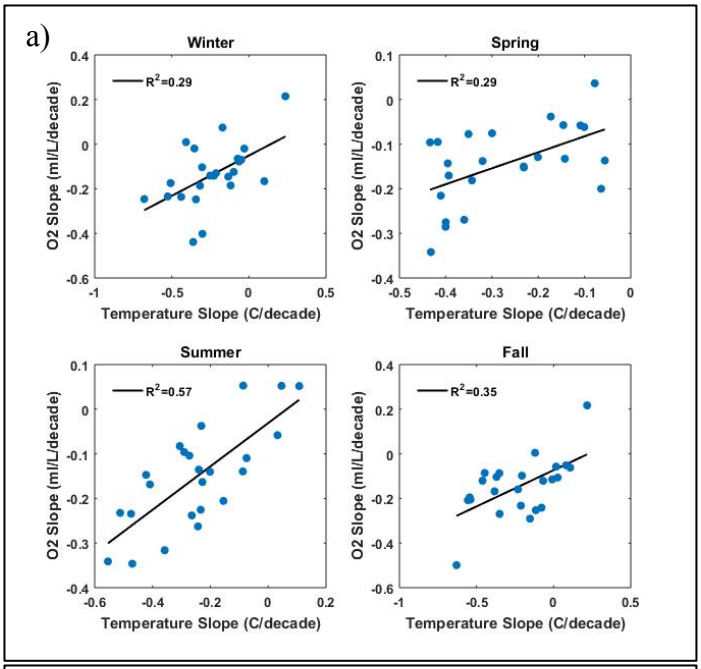
a)
Winter
R²=0.29
Spring
R²=0.29
Summer
R²=0.57
Fall
R²=0.35
O2 Slope (ml/L/decade)
Temperature Slope (C/decade)

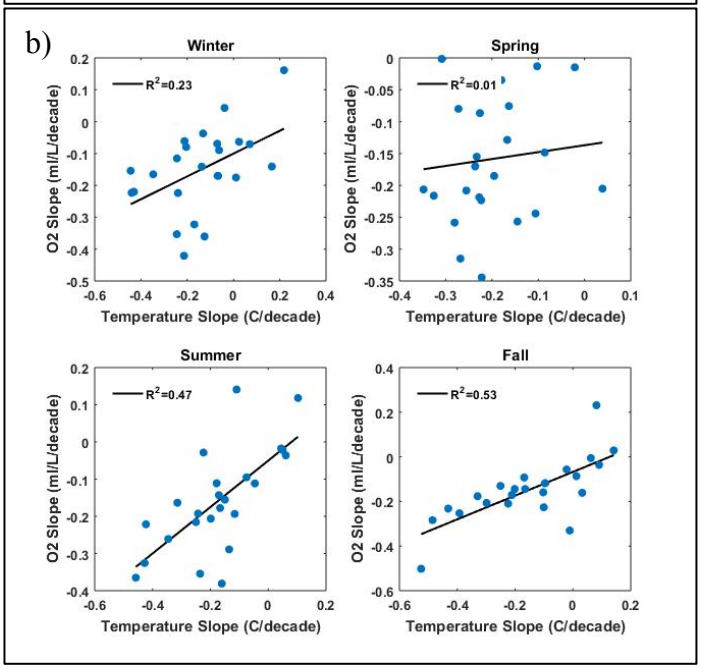
b)
Winter
R²=0.23
Spring
R²=0.01
Summer
R²=0.47
Fall
R²=0.53
O2 Slope (ml/L/decade)
Temperature Slope (C/decade)

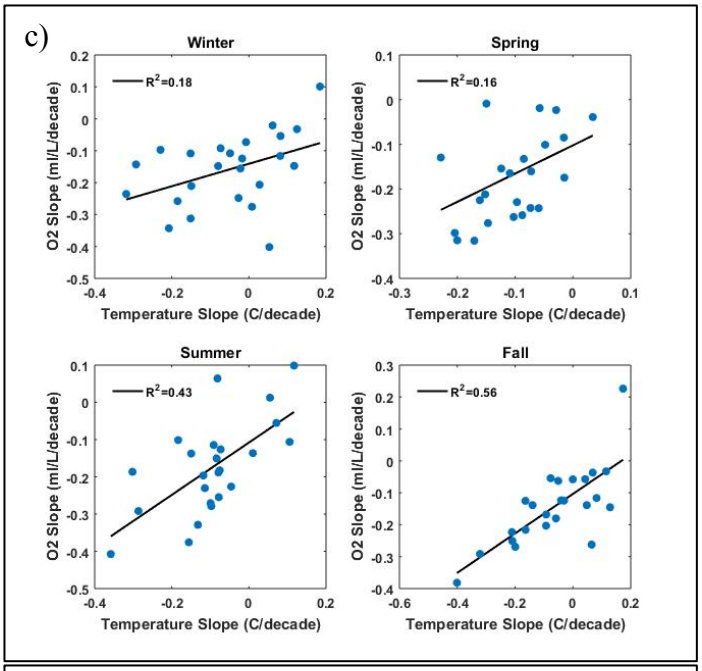
c)
Winter
R²=0.18
Spring
R²=0.16
Summer
R²=0.43
Fall
R²=0.56
O2 Slope (ml/L/decade)
Temperature Slope (C/decade)

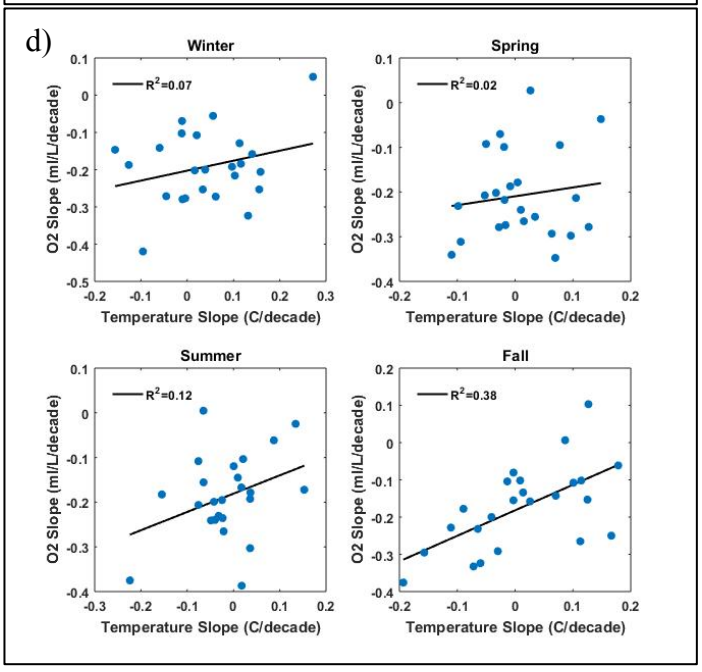
d)
Winter
R²=0.07
Spring
R²=0.02
Summer
R²=0.12
Fall
R²=0.38
O2 Slope (ml/L/decade)
Temperature Slope (C/decade)

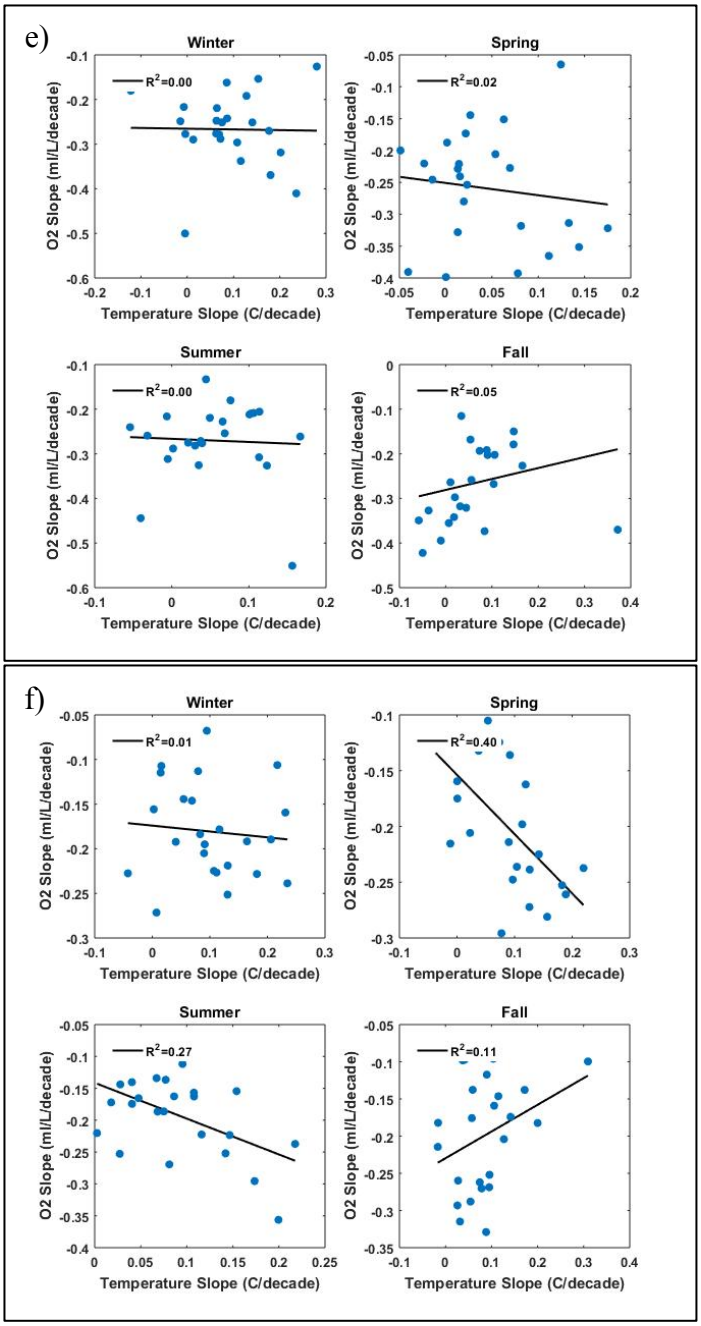


**Figure 18.** Seasonal comparison of oxygen concentration trends to temperature trends on isopycnals displaying potential densities of a) 25.5, b) 25.75, c) 26, d) 26.25, e) 26.5, and f) 26.75 kg/m$^3$. Trends of variables are calculated using Sen's slope. Each point represents the oxygen and temperature values of an individual station at the specified isopycnal. The black linear trend line represents a least-square regression between the two variables, and its $R^2$ value is given.

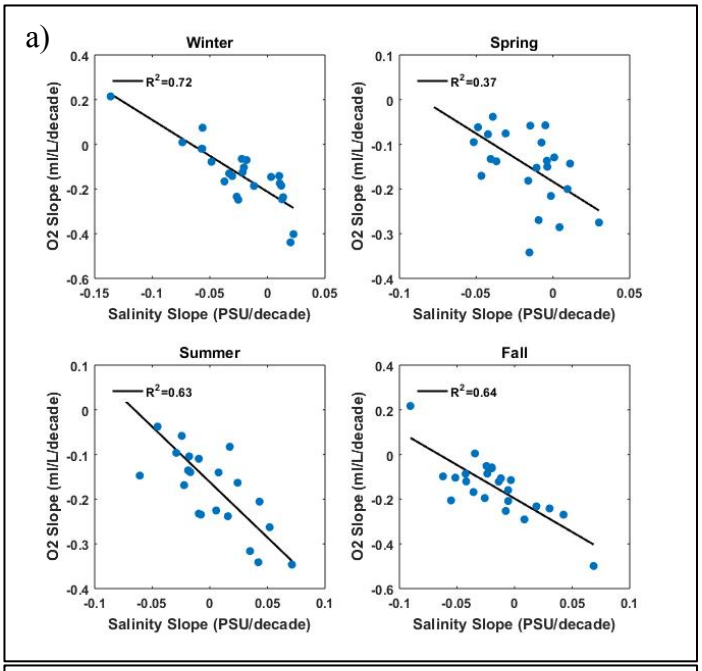
a)
Winter
$R^2$=0.72
Spring
$R^2$=0.37
Summer
$R^2$=0.63
Fall
$R^2$=0.64
O2 Slope (ml/L/decade)
Salinity Slope (PSU/decade)

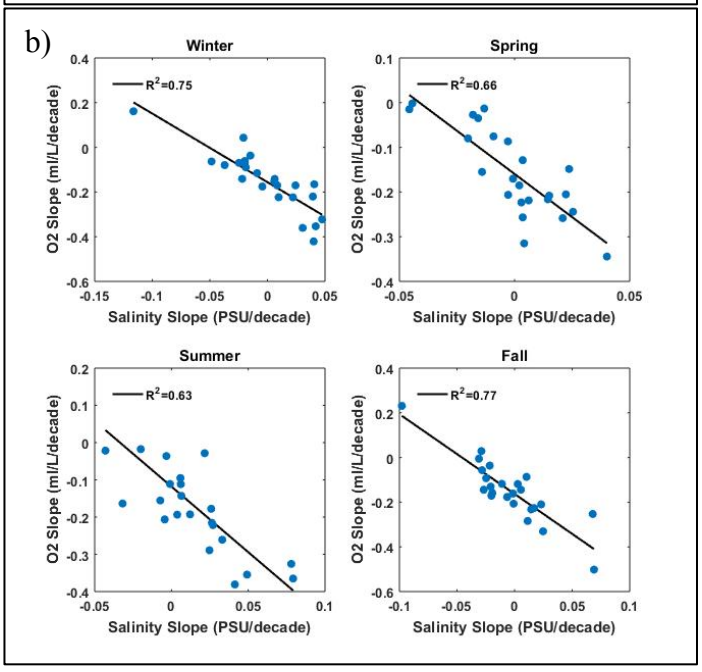
b)
Winter
$R^2$=0.75
Spring
$R^2$=0.66
Summer
$R^2$=0.63
Fall
$R^2$=0.77
O2 Slope (ml/L/decade)
Salinity Slope (PSU/decade)

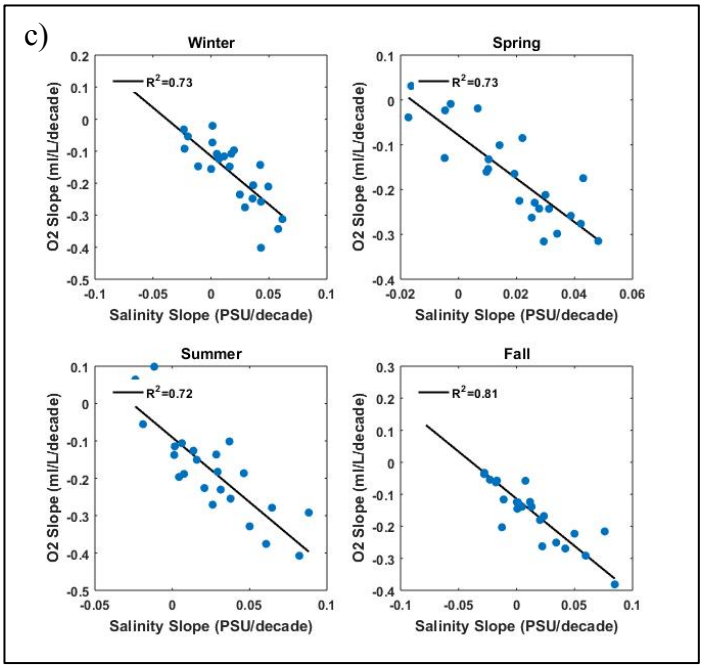
c)
Winter
$R^2$=0.73
Spring
$R^2$=0.73
Summer
$R^2$=0.72
Fall
$R^2$=0.81
O2 Slope (ml/L/decade)
Salinity Slope (PSU/decade)

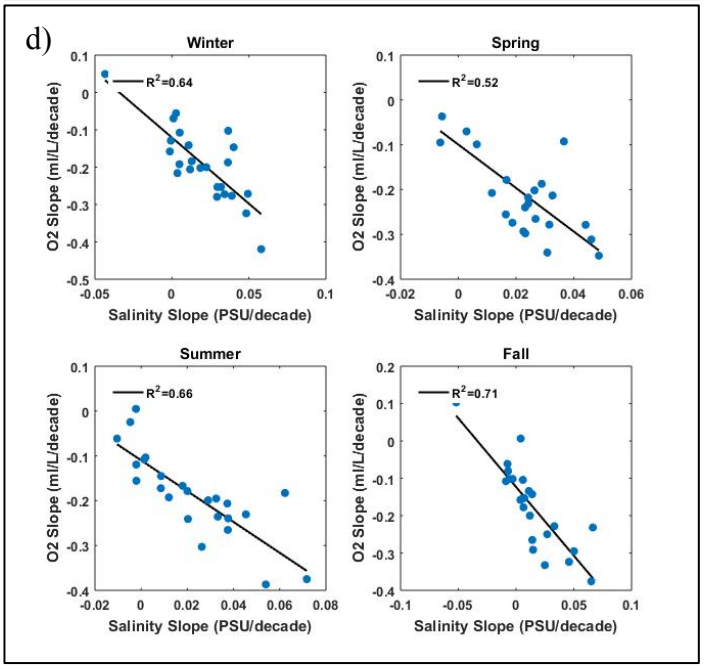
d)
Winter
$R^2$=0.64
Spring
$R^2$=0.52
Summer
$R^2$=0.66
Fall
$R^2$=0.71
O2 Slope (ml/L/decade)
Salinity Slope (PSU/decade)

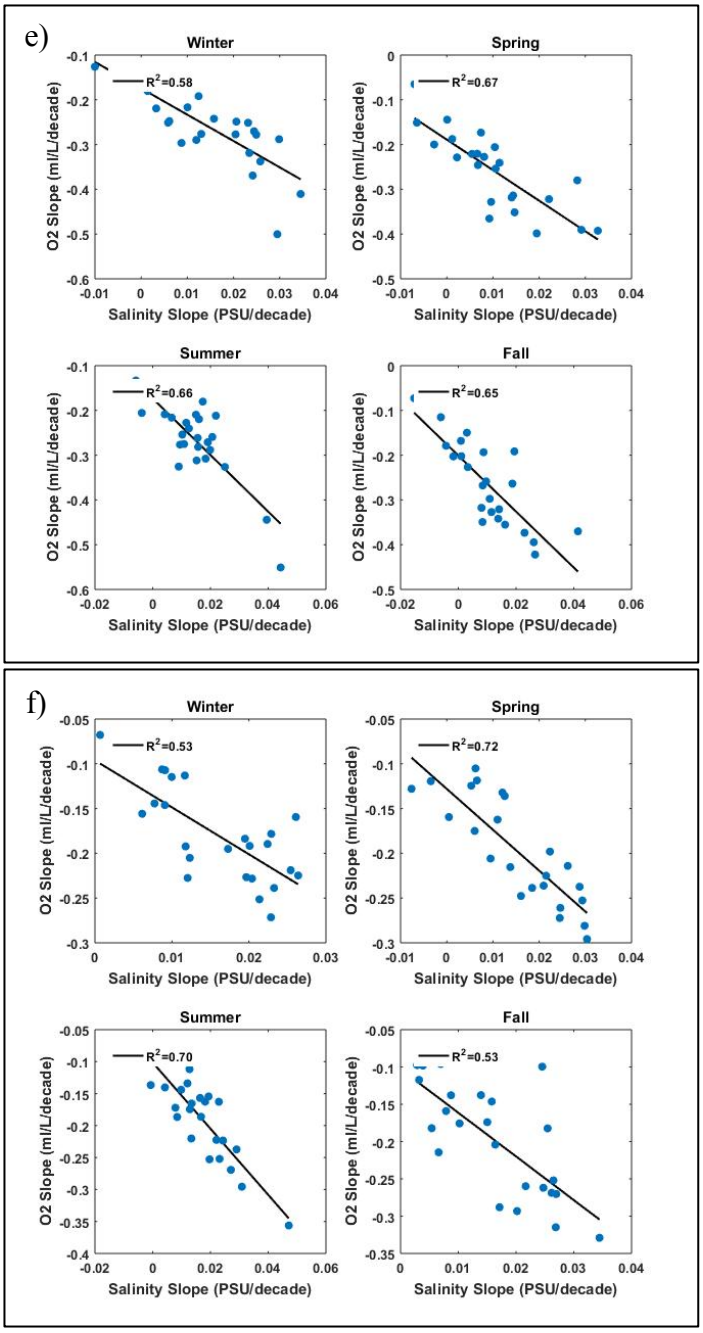


**Figure 19.** Seasonal comparison of oxygen concentration trends to salinity trends on isopycnals displaying potential densities of a) 25.5, b) 25.75, c) 26, d) 26.25, e) 26.5, and f) 26.75 kg/m$^3$. Trends of variables are calculated using Sen's slope. Each point represents the oxygen and salinity values of an individual station at the specified isopycnal. The black linear trend line represents a least-square regression between the two variables, and its $R^2$ value is given.

# DISCUSSION

## Levels of Maximum Deoxygenation

The rate of deoxygenation off the coast of southern California varies with depth, location, and density, with maximum rates of deoxygenation seen at the approximate depth of 200 meters and the potential density of 26.5 kg/m$^3$ (Fig. 10,11). At these values, two observations of the system can be made. First, the 26.5 kg/m$^3$ isopycnal often oscillates near or around 200 meters in depth (Fig. 3). Second, isopycnals can display as strong of trends in deoxygenation as seen with depth, primarily noticeable between the 200-meter depth level and 26.5 kg/m$^3$ isopycnal (Fig. 10,11). Considered together, shoaling of isopycnals does not appear to be the primary driver of oxygen decline recorded within this system, as peak deoxygenation does not decrease when viewing isopycnals. That being said, differences in cross-shore and latitudinal patterns between density-interpolated and depth-interpolated trends indicate that shoaling does shape spatially-apparent trends in deoxygenation (Fig. 10,11).

Several papers have recorded this subsurface deoxygenation maximum off the coast of California, although its exact depth varies by methodology and location of focus (Meinvielle and Johnson, 2013 & Bograd *et al*., 2015). Most notably, the work here followed a similar methodology of Bograd *et al.* (2008), mapping oxygen trends in CalCOFI data over spatial layouts of equal depth. The results here verify many of the patterns presented by Bograd *et al.* (2008). These authors (2008), noticed a similar mid-water peak in deoxygenation; however, absence of the 300-meter depth data in our study may have contributed to difference of the depth of peak deoxygenation from 300 meters

to 200 meters. The waters of the feature in question are classified as part of the California Undercurrent, which appears in the density range of 26.4 to 26.6 (Nam *et al*., 2015).

Along the 26.5 kg/m$^3$ isopycnal, we observe positive trends in both temperature and salinity (Fig. 7,9). In previous studies, variation in the spiciness, a composite variable calculated from temperature and salinity, have been shown to be increasing in this system (Meinvielle and Johnson, 2013 & Bograd *et al*., 2015), as well as other regions within the California current system (Meinvielle and Johnson, 2013). The California Undercurrent derives water primarily from Pacific Equatorial water (Lynn and Simpson, 1987), which dilutes into Pacific Subarctic Upper water as it advects poleward (Lynn and Simpson, 1990; Meinvielle and Johnson, 2013). As Pacific Equatorial water shows increased salinity and temperature compared to Pacific Subarctic Upper water (Lynn and Simpson, 1987), recent trends have suggested an increase in Pacific Equatorial water throughout the California Undercurrent (Meinvielle and Johnson, 2013). As Pacific Equatorial waters also display low oxygen levels (Lynn and Simpson, 1987), increased presence would be expected to lower dissolved oxygen in the California Undercurrent (Meinvielle and Johnson, 2013), as we observe in this study.

Altogether, through increased temperature and salinity, we observed the component changes of this previously recorded increase in spiciness. As noted previously (Meinvielle and Johnson, 2013), we observed this trend in conjunction with diminished oxygen concentrations. Our results therefore agree that increases in Pacific Equatorial source waters play a major factor in influencing the deoxygenation trends of this region.

Spatial deoxygenation trends above the 26.5 kg/m$^3$ isopycnal (<200 meters)

Depth-based and density-based maps of oxygen concentration trends depict two separate patterns. First, depth-based oxygen trends show distinct cross-shelf differences in deoxygenation, with greater deoxygenation rates nearshore (Fig. 10). Second, density-based oxygen trends depict latitudinal differences in deoxygenation at isopycnals, with greater deoxygenation present in the northern lines, 80 and 83.3, and lower deoxygenation in southern lines, 86.7 and 93.3 (Fig. 11).

Nearshore maxima in deoxygenation rates in depth-based plots (Fig. 10) correspond to expected patterns from upwelling. These oxygen trends are apparent between the 30-meter and 100-meter depth spatial plots of oxygen trends and exist both inside and outside the Bight (Fig. 10b-d). These patterns correspond to similar observations by Bograd *et al*. (2008). Upwelling depth within the region can vary over time; however, recent literature places the upwelling depth in the vicinity of the California Undercurrent at depths approaching 200 meters (Chhak and Di Lorenzo, 2007 & Meinvielle and Johnson, 2013). As a result, shoaling of isopycnals and upwelling of California Undercurrent waters distribute the heightened deoxygenation trends into upper waters, especially nearshore (Bograd *et al*., 2008). Climatological plots of potential density suggest that seasonal upwelling occurs within all lines of this study (Fig. 3). Although upwelling peaks in the spring for each line, climatological means point to shallower isopycnals at nearshore stations as a consistent year-round feature (Fig. 3). As depth-based plots do not standardize values relative to isopycnals, oxygen-depleted waters seen across isopycnals occur at different depths relative to cross-shelf position. These differences in isopycnal depth contribute to retention of cross-shore trends in

deoxygenation driven by vertical movement of California Undercurrent waters at nearshore stations.

The strength of these nearshore trends likely also represents trends in upwelling strength in addition to composition of upwelled water. As indicated by the upwelling indices calculated from NOAA's Pacific Fisheries Environmental Laboratory (PFEL) using coastal wind stresses north of the Bight, the strength of upwelling has been increasing within this region from 1988 to 2016 (Fig. 20a). With increased index, a greater volume of water is expected to upwell (PFEL), carrying more low-oxygen water to the surface and exacerbating the deoxygenation trend. Within the Bight, the upwelling index, although positive, is about four times smaller, suggesting trends in wind forcing primarily influence deoxygenation in the region outside the Bight (Fig. 20b).

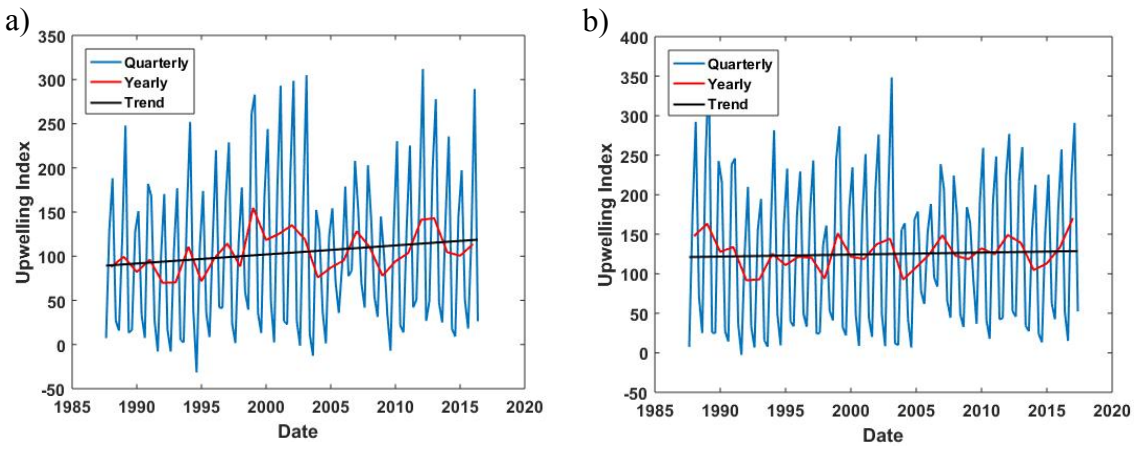


**Figure 20.** Upwelling indices calculated by the Pacific Fisheries Environmental Laboratory from 1988 to 2016 at a) 36 N 122 W and b) 33 N 119 W. Upwelling index values show units of $m^3$/sec/100 m. Linear trends derive from least-squared fits of the quarterly data. For 36 N, the trend is 10.2 $m^3$/sec/100 m/decade, and, for 33 N, the trend is 2.5 $m^3$/sec/100 m/decade.

Despite nearshore elevations of deoxygenation persisting throughout most of the year, the trends appear reduced or absent during spring, especially within the upper 50 meters of the water column (Fig. 10). While heightened upwelling in this period would

otherwise suggest strong deoxygenation trends, biological properties, namely photosynthesis, likely overwhelm the physical drivers at this time. As shown in Haskell II *et al*. (2017) during a study proximate to a nearshore CalCOFI station within the Bight (station 90 40), this region displays a pronounced spring phytoplankton bloom event. These authors show that net oxygen production by phytoplankton reaches levels nearly 200 mmol/$m^2$/d greater than seen in fall or winter months, when these values approach zero mmol/$m^2$/d (Haskell II *et al*., 2017). As these elevated levels of oxygen form from phytoplankton photosynthesis fed by nutrients carried by upwelled waters, they offset the deoxygenation trends seen throughout the rest of the year similarly caused by upwelled waters. It should be noted that subsequent decomposition of blooms will likely reduce oxygen within a system, as well; however, this decrease would occur later in the spring and likely be advected away from oxygen patterns observed here (Connolly *et al*., 2010).

Density-based latitudinal patterns in deoxygenation rates likely coincide with recirculation and associated downwelling in the Southern California Bight. Latitudinal patterns appear most strongly down to the 26.0 kg/$m^3$ isopycnal (Fig. 11). As discussed above, the Bight has quite different circulation patterns compared to northern regions; most notably, the equatorward California Current separates from the coastline at the Bight, generating a recirculation pattern within the Bight (Bray *et al.*, 1999). This phenomenon generates poleward flow (Bray *et al.*, 1999) indicative of downwelling of upper waters within the Bight. Waters that have experienced reoxygenation and photosynthesis transfer elevated oxygen concentrations to lower isopycnals as waters are subducted, offsetting deoxygenation trends observed within the latitudes of the Bight. As the northern lines have a more persistent equatorward flow (Bray *et al.*, 1999),

downwelling, such as generated by poleward winds, would remain smaller than in southern latitudes.

As with depth-based cross-shelf patterns, these latitudinal trends occur mostly outside the spring season (Fig. 11). During spring, Bray *et al.* (1999) notes the California Current is nearer to the California coast throughout the Bight with an associated lack of recirculation within the Bight. This lack of recirculation prevents the anticipated downwelling of other seasons, while equatorward flow stimulates upwelling (Bray *et al.*, 1999).

## Oxygen-Hydrography Temporal Correlations

Comparisons between hydrographic variables and oxygen concentration returned considerably lower correlation values when viewed at standard depths than when viewed on isopycnals (Fig. 16-19). As the removal of isopycnal variability results in higher correlation, this suggests that a sizable proportion of the oxygen trend in this system stems from trends in water properties and water transport, such as source water advection and upwelling. This observation agrees with previous conclusions of the importance of California Undercurrent source waters in driving changes in oxygen concentrations (Meinvielle and Johnson, 2013, Bograd *et al*., 2015). Biological impacts likely reduce the observed correlations between hydrographic trends and oxygen trends, as rates of oxygen production and consumption also serve to alter the oxygen structure of the ocean (Connolly *et al*., 2010 & Haskell II *et al*., 2017).

Despite the overall lower correlation values when comparing oxygen and hydrographic variables at standard depths, below the depth of upwelling, salinity begins showing reasonable correlation with oxygen (Fig. 17). Below the depth of upwelling,

interannual variability becomes smaller than seen in upper waters (Fig. 12-15). Within the California current system, three primary basin-scale climatic processes induce temporal variability: El Niño Southern Oscillation (ENSO), Pacific Decadal Oscillation (PDO), and North Pacific Gyre Oscillation (NPGO) (Di Lorenzo *et al*., 2008; Jacox *et al*., 2015). Of these three, ENSO acts on an interannual scale through shifts in the atmospheric pressure cells over the North Pacific, resulting in changing wind patterns and upwelling over our study area (Jacox *et al*., 2015). During El Niño events and La Niña events, wind relaxations result in diminished upwelling and wind intensification results in increased upwelling, respectively (Jacox *et al*., 2015); however, La Niña generally shows smaller magnitudes than does El Niño (Jacox *et al*., 2015). These upwelling related responses generate isopycnal movement primarily above 200 meters (Nam *et al*., 2015), the depth from which water is drawn to toward the surface. Below this depth, the confounding isopycnal variability minimizes (Nam *et al*., 2015), allowing hydrographic correlations to strengthen.

In both depth-based and density-based comparisons, salinity increases track oxygen decreases at or below the upwelling interface (Fig. 17,19). Below levels directly impacted by upwelling, longer scale trends, such as decadal scale shifts in source water, comprise a more significant portion of variability as interannual trends subside. The PDO categorizes a decadal pattern in sea surface temperatures; whereas, the NPGO tracks decadal-scale shifts in upwelling-favorable wind forcing (Di Lorenzo *et al*., 2008). As an increase in upwelling corresponds with increased volumes of source water drawn into the California Undercurrent (Meinvielle and Johnson, 2013), it follows that the NPGO would strongly influence many oceanic trends related to source water

characteristics, such as the oxygen concentrations and salinities of the California Undercurrent. In fact, Di Lorenzo *et al*. (2008) have displayed upper ocean oxygen concentrations and surface salinities tracking best with NPGO, unlike surface temperatures which follow PDO. The results of our study suggest similar patterns at depth, with the correlation between oxygen and salinity likely occurring due to shared decadal forcing patterns. As one would expect under this interpretation, temperature deviates within this region, perhaps due to different decadal patterns (Di Lorenzo *et al*., 2008) or confounding variables, such as global ocean warming patterns.

While little correlation is seen at depth interfaces within the upper ocean, relationships become visible when trends are restricted to isopycnals (Fig. 18,19). Above the California Undercurrent, temporal trends on isopycnals see substantial shaping from upwelling, as indicated by predominantly negative temperature trends as colder, deeper water mixes into shallower isopycnals (Fig. 7). As a result of upwelling, variables with values characteristic of a source water, including oxygen concentration and spiciness, will often show corresponding trends (Meinvielle and Johnson, 2013). In effect, the low oxygen, high salinity, and low temperature signals all mix upward under the influence of upwelling. Where the upwelling changes strength over time and/or source water properties change over time, trends in variables are generated, such as the elevated deoxygenation seen in the lines 80 and 83 (Fig. 11). Where upwelling trends are weaker, such as in the Bight (Fig. 20), deoxygenation changes may be driven by these weakened upwelling trends coupled with advection of lower oxygen water formed in upstream areas of the California Current (Bray *et al*., 1999 & Schneider *et al*., 2005). In total, while decadal patterns do not align between temperature and oxygen, the shared interannual

forcing of ENSO results in increased correlation between temperature and oxygen above the California Undercurrent (Fig. 18,19). The potential implications of heat flux with the atmosphere likely limit the correlation strength, as suggested by Schneider *et al*. (2005). Meanwhile, the coupled ENSO and NPGO influences on salinity and oxygen concentration cause strongly corresponding trends to appear over this density range. Correlation with salinity, due to stronger coupling in their forcing, exceeds that of temperature, suggesting that trends in salinity serve as a more optimal indicator of oxygen trends between potential densities of 25.5 and 26.25 $kg/m^3$. At or above densities of 26.5 $kg/m^3$, lack of correlation with temperature implicates salinity once again as a better predictive variable.

It should be noted that, due to the paired relationship of salinity and temperature in determining the density of sea water, one would expect temperature and salinity to show similar correlations with oxygen on isopycnals. The lack of this similarity in our study likely stems either from error inherent in our linear interpolation or, possibly, from the use of potential density in calculating isopycnals. Potential densities correct for pressure-based changes in temperature, using a variable called potential temperature in the calculation. As temperature transforms non-linearly to potential temperature, this transformation may ultimately result in a disconnect in the correlation of temperature and salinity on the isopycnals used for this study.

# CONCLUSIONS

Through recurrence of a previously observed deoxygenation maximum in the California Undercurrent, coupled with observed increases in temperature and salinity representative of source waters, our results support the existing literature indicating that substantial decreases in oxygen in this region stem from increased influences of Pacific Equatorial waters. These shifts in the California Undercurrent then propagate throughout the system through upwelling, generating strong nearshore deoxygenation visible at depth interfaces. Meanwhile, regional, ephemeral downwelling within the Bight suppresses southern deoxygenation events along isopycnals. While both temperature and salinity trends show signs of correlating with oxygen concentration trends, salinity correlation, driven by shared forcing by ENSO and NPGO with oxygen and absence of the ocean-atmosphere exchange seen in temperature, appears to dominate. As such, salinity trends, specifically along isopycnals, serve as a better predictor of oxygen trends within this system.

# BIBLIOGRAPHY


Bograd, S.J., Castro, C.G., Di Lorenzo, E., Palacios, D.M., Bailey, H., Gilly, W., Chavez, F.P. 2008. Oxygen declines and the shoaling of the hypoxic boundary in the California Current. *Geophysical Research Letters*. 35(12).

Bograd, S.J., Buil, M.P., Di Lorenzo, E., Castro, C.G., Schroeder, I.D., Goericke, R., Anderson, C.R., Benitez-Nelson, C., Whitney, F.A. 2015. Changes in source waters to the Southern California Bight. *Deep Sea Research Part II: Topical Studies in Oceanography*. 112:42-52.

Bray, N.A., Keyes, A., Morawitz, W.M.L. 1999. The California Current System in the Southern California Bight and the Santa Barbara Channel. *Journal of Geophysical Research*. 104(C4):7695-7714.

Caldiera, R.M.A. and Marchesiello, P. 2002. Ocean response to wind sheltering in the Southern California Bight. *Geophysical Research Letters*. 29(13):13-1-13-4.

[CalCOFI] Calfornia Cooperative Ocean Fisheries Investigation. 1611 Introduction. [Internet]; 2016 [cited 2018 Apr 23]. 6 p. Available from http://calcofi.org/data/data_reports/2016/1611INTR.pdf

[CalCOFI] Calfornia Cooperative Ocean Fisheries Investigation. Data Report: Physical, Chemical and Biological Data. [Internet]; 1989 [cited 2018 Apr 23]. 80 p. Available from http://calcofi.org/data/data_reports/1980s/pdf/8801final.pdf

Chhak, K. and Di Lorenzo, E. 2007. Decadal variations in the California Current upwelling cells. *Geophysical Research Letters*. 34(14).

Connolly, T.P., Hickey, B.M., Geier, S.L., Cochlan, W.P. 2010. Processes influencing seasonal hypoxia in the northern California Current System. *Journal of Geophysical Research*. 115(C3).

Di Lorenzo, E., Schneider, N., Cobb, K.M., Franks, P.J.S., Chhack, K., Miller, A.J., McWilliams, J.C., Bograd, S.J., Arango, H., Curchitser, E., Powell, T.M., Riviére, P. 2008. North Pacific Gyre Oscillation links ocean climate and ecosystem change. *Geophysical Research Letters*. 35(8).

Gilly, W. F., Beman, J.M., Litvin, S.Y., Robison, B.H. 2013. Oceanographic and Biological Effects of Shoaling of the Oxygen Minimum Zone. *Annual Review of Marine Science*. 5:393-420.

Haskell II, W.Z., Prokopenko, M.G., Hammond, D.E., Stanley, R.H.R., Sandwith, Z.O. 2017. Annual cyclicity in export efficiency in the inner Southern California Bight. *Global Biochemical Cycles*. 31:357-376. 120:1691-1702.

Jacox, M.G., Fiechter, J., Moore, A.M., Edwards, C.A. 2015. ENSO and the California Current coastal upwelling response. *Journal of Geophysical Research: Oceans*

Lynn, R.J. and Simpson, J.J. 1987. The California Current System: The Seasonal Variability of its Physical Characteristics. *Journal of Geophysical Research*. 92(C12):12947-12966.

Lynn, R.J. and Simpson, J.J. 1990. The Flow of the Undercurrent Over the Continental Borderland off Southern California. *Journal of Geophysical Research*. 95(C8):12995-13008.

McClatchie, S., Goericke, R. Cosgrove, R., Auad, G., Vetter, R. 2010. Oxygen in the Southern California Bight: Multidecadal trends and implications for demersal fisheries. *Geophysical Research Letters*. 37(19).

Meinvielle, M. and Johnson, G.C. 2013. Decadal water-property trends in the California Undercurrent, with implications for ocean acidification. *Journal of Geophysical Research: Oceans*. 118(12).

Nam, S., Takeshita, Y., Frieder, C.A., Martz, T. Ballard, J. 2015. Seasonal advection of Pacific Equatorial Water alters oxygen and pH in the Southern California Bight. *Journal of Geophysical Research: Oceans.* 120(8).

[PFEL] Pacific Fisheries Environmental Laboratory. Coastal Upwelling Indices. [Internet]. [2018; cited 2018 Apr 21]. Available from https://www.pfeg.noaa.gov/products/PFEL/modeled/indices/upwelling/NA/upwell_menu_NA.html

Schneider, N., Di Lorenzo, E., Niiler, P.P. 2005. Salinity Variations in the Southern California Current. *Journal of Physical Oceanography*. 35(8):1421-1436.

Stramma, L. Schmidtko, S., Levin, L.A., Johnson, G.C. 2010. Ocean oxygen minima expansions and their biological impacts. *Deep-Sea Research I*. 57:587-595.

# APPENDIX

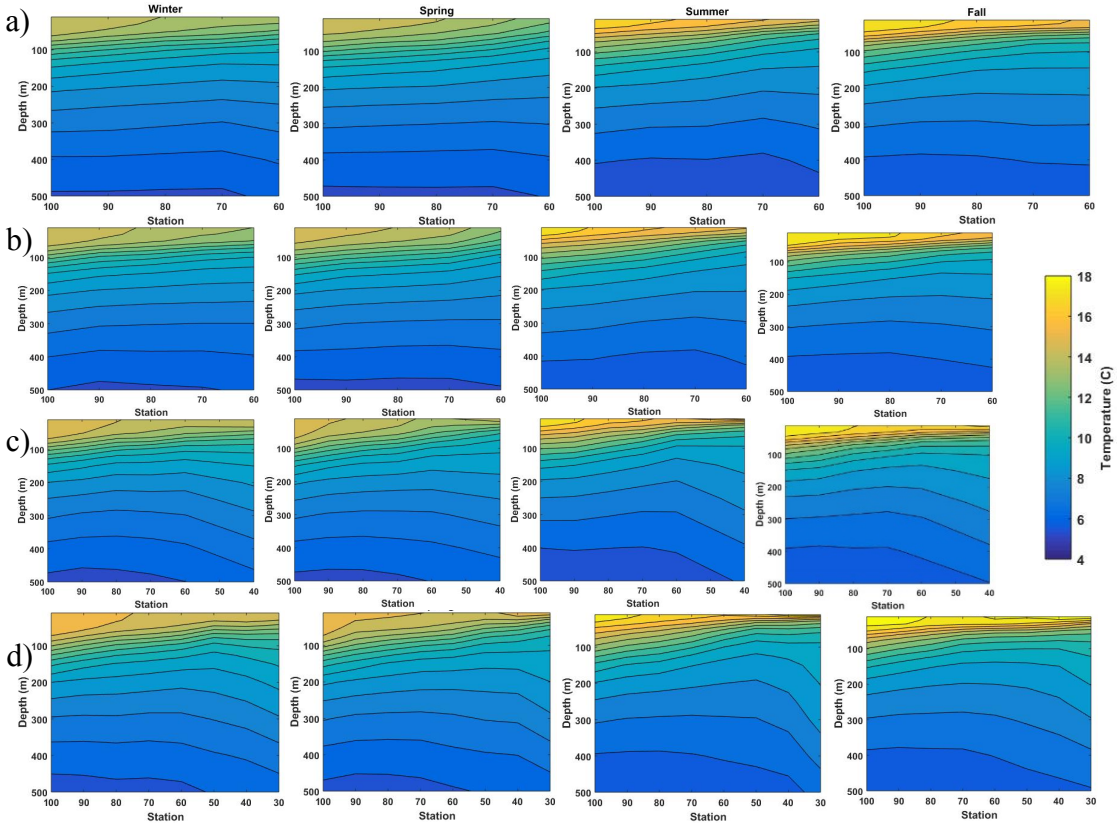


**Figure A1.** Climatological, seasonal contours of cross-shelf vertical temperature structure in the upper 500 meters from 1950 to 2016 along lines a) 80, b) 83.3, c) 86.7, and d) 93.3.

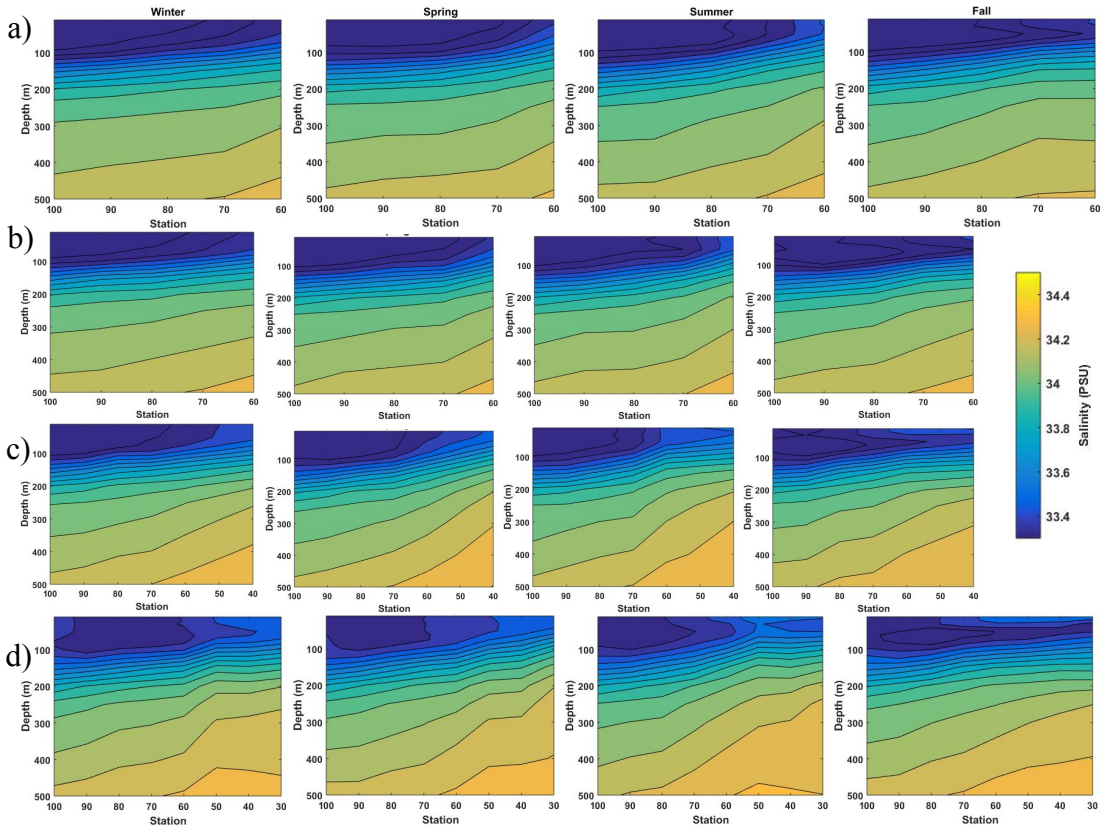


**Figure A2.** Climatological, seasonal contours of cross-shelf vertical salinity structure in the upper 500 meters from 1950 to 2016 along lines a) 80, b) 83.3, c) 86.7, and d) 93.3.


**Figure A3.** Seasonal time series of depth of isopycnals over the period of 1988 to 2016 at three stations on line a) 80, b) 83.3, c) 86.7, and d) 93.3. Isopycnal values represent potential densities. From left to right, stations move cross-shelf away from shore, with the leftmost station being the station closest to shore utilized in this study.

# AUTHOR'S BIOGRAPHY

Born in Greenville, South Carolina, Todd X. Thoman moved to Spring Grove, Pennsylvania at an early age. Here, he graduated from Spring Grove High School in May 2014. During his time at the University of Maine, Todd majored in marine sciences with a concentration in marine physical sciences/oceanography. Todd was inducted into Phi Beta Kappa in 2016 and graduated from the University of Maine in May 2018.

Following graduation, Todd will begin a master's degree at the University of Delaware in the Physical Ocean Sciences and Engineering program. Ultimately, Todd aims to achieve a doctoral degree within the realm of physical oceanography.